Geochemistry Geophysics Geosystems G3

Article
Volume 13, Number 9
19 September 2012
Q09008, doi:10.1029/2012GC004150
ISSN: 1525-2027

Published by AGU and the Geochemical Society

Carbon cycle dynamics following the end-Triassic mass extinction: Constraints from paired $\delta^{13}C_{carb}$ and $\delta^{13}C_{org}$ records

Aviv Bachan
Department of Geological and Environmental Sciences, Stanford University, Stanford, California 94305, USA (avivbd@stanford.edu)

Bas van de Schootbrugge and Jens Fiebig
Institute of Earth Sciences, Department of Paleontology, Goethe Universität Frankfurt am Main, Frankfurt DE-60439, Germany (van.de.schootbrugge@em.uni-frankfurt.de; jens.fiebig@em.uni-frankfurt.de)

Christopher A. McRoberts
Department of Geology, State University of New York College at Cortland, Cortland, New York 13045, USA (mcroberts@cortland.edu)

Gloria Ciarapica
Dipartimento di Scienze della Terra, Università degli Studi di Perugia, Piazza Università, Perugia IT-06100, Italy

Jonathan L. Payne
Department of Geological and Environmental Sciences, Stanford University, Stanford, California 94305, USA (jlpayne@stanford.edu)

[1] Constraining the carbon isotopic changes associated with the end-Triassic mass extinction is key to understanding the causes of the extinction and dynamics of recovery from it. Yet the pattern and timing of $\delta^{13}C$ variation surrounding the extinction remain poorly constrained. Here we present close to 1000 new $\delta^{13}C$ measurements from six newly sampled sections in Italy. We observe a sharp negative excursion in $\delta^{13}C_{carb}$ coincident with the disappearance of the Triassic fauna, and two positive excursions above it. The negative $\delta^{13}C_{carb}$ excursion in these sections does not occur in $\delta^{13}C_{org}$ suggesting a possible diagenetic origin. In contrast, the interval of elevated $\delta^{13}C$ occurs in both carbonate and organic carbon, suggesting that it is likely to be a primary feature. The positive excursions in the Lombardy Basin (southern Alps) and Mt. Cefalo (southern Apennines) appear to be time correlative on the basis of their position above the disappearance of characteristically Triassic biota. However, it is less certain that they are time correlative with positive excursions in other sections worldwide, as few options exist that honor both bio- and chemostratigraphy. Nonetheless, similarity to other events that are interpreted as global, as well as carbon cycle considerations, suggest that the isotopic enrichment is best interpreted to reflect a shift in the isotope composition of the global surface carbon reservoir. Our data indicate that perturbation of the global carbon cycle was not confined to the immediate vicinity of the extinction interval, but rather persisted for substantial length of geologic time afterwards.

Components: 8500 words, 15 figures.

Keywords: Triassic-Jurassic boundary; carbon cycle dynamics; carbon isotopes; end-Triassic mass extinction.

Index Terms: 0428 Biogeosciences: Carbon cycling (4806); 0454 Biogeosciences: Isotopic composition and chemistry (1041, 4870); 0459 Biogeosciences: Macro- and micropaleontology (3030, 4944).

Received 19 March 2012; **Revised** 25 July 2012; **Accepted** 7 August 2012; **Published** 19 September 2012.

Bachan, A., B. van de Schootbrugge, J. Fiebig, C. A. McRoberts, G. Ciarapica, and J. L. Payne (2012), Carbon cycle dynamics following the end-Triassic mass extinction: Constraints from paired $\delta^{13}C_{carb}$ and $\delta^{13}C_{org}$ records, *Geochem. Geophys. Geosyst.*, *13*, Q09008, doi:10.1029/2012GC004150.

1. Introduction

[2] Stable carbon isotopes have been widely used to investigate the nature of biotic and physical events leading up to, and following, the end-Triassic mass extinction. A negative δ^{13}C excursion coincident with the disappearance of Triassic biota occurs in multiple locations globally (British Columbia [*Ward et al.*, 2001, 2004; *Williford et al.*, 2007], Hungary [*Pálfy et al.*, 2001], the UK [*Hesselbo et al.*, 2002; *Korte et al.*, 2009; *Ruhl et al.*, 2010a; *Clémence et al.*, 2010], Nevada [*Guex et al.*, 2004; *Ward et al.*, 2007], Austria [*Morante and Hallam*, 1996; *McRoberts et al.*, 1997; *Kürschner et al.*, 2007; *Ruhl et al.*, 2009; *Bonis et al.*, 2010; *Ruhl et al.*, 2010b, 2011], Japan [*Kuroda et al.*, 2010], Denmark [*Lindström et al.*, 2012], and Italy [*Galli et al.*, 2005]). The negative shift has been interpreted as the result of a productivity collapse [*Ward et al.*, 2001], the injection of ^{13}C depleted CO_2 associated with the emplacement of the Central Atlantic Magmatic Province (CAMP) [*Beerling and Berner*, 2002], and/or methane hydrate release [*Hesselbo et al.*, 2002; *Ruhl et al.*, 2011]. The negative excursion is followed by a protracted interval of ^{13}C enrichment at a number of sites. Large positive δ^{13}C excursions occur in the Hettangian of Queen Charlotte Islands, Canada [*Williford et al.*, 2007], northern Italy [*van de Schootbrugge et al.*, 2008], and New York Canyon, Nevada [*Bartolini et al.*, 2012]. The enrichment has been interpreted to result from a volcanically driven increase in pCO_2, which raised global temperatures, nutrient delivery to the oceans, and the burial flux of organic carbon [*van de Schootbrugge et al.*, 2008; *Bartolini et al.*, 2012].

[3] Yet, many aspects of the carbon isotope record from the latest Triassic and lowermost Jurassic remain poorly constrained, particularly regarding local versus global influences on the δ^{13}C record. There is a strong correlation between the relative abundances of the palynomorph types and the overall isotopic composition of bulk organic carbon [*van de Schootbrugge et al.*, 2008; *Bonis et al.*, 2009], suggesting a strong compositional control on bulk $\delta^{13}C_{org}$ in some cases. The δ^{13}C signature of carbonate rocks shows a correlation with facies: in northern Italy the peak of the prolonged positive excursion appears in the shallowest facies [*van de Schootbrugge et al.*, 2008]. Lastly, the lack of paired $\delta^{13}C_{org}$ and $\delta^{13}C_{carb}$ records from the same samples and sections contributes substantially to the uncertainties in stratigraphic correlation, and hence interpretation of the underlying global carbon cycle behavior [*Bartolini et al.*, 2012].

[4] In order to improve our understanding of end-Triassic and lowermost Jurassic carbon cycle dynamics, we present extended, paired organic and carbonate δ^{13}C curves from newly sampled sections in the southern Alps and the central and southern Apennines of Italy (Figure 1).

2. Geologic Setting

[5] Despite the disruption caused by Cenozoic orogenesis, a few major paleogeographic domains are known from the Upper Triassic and Lower Jurassic of Italy: a deep ocean separated Italy from Africa to the south (the Ionian arm of the Tethys) [*Passeri et al.*, 2005; *Ciarapica and Passeri*, 2005; *Bertinelli et al.*, 2005], and a series of shallow basins connected Italy with Europe to the north [*Jadoul et al.*, 2005] and west [*Ciarapica and Passeri*, 1980]. The interior was divided into various topographic highs with intraplatform basins interspersed between them [*Adamoli et al.*, 1990; *Zappaterra*, 1994; *Bertinelli et al.*, 2004]. Carbonates and evaporites accumulated in shallow waters, while carbonate muds, cherty limestones, cherts, and shales were deposited in the often dysoxic intraplatform basins [*Ciarapica*, 2007].

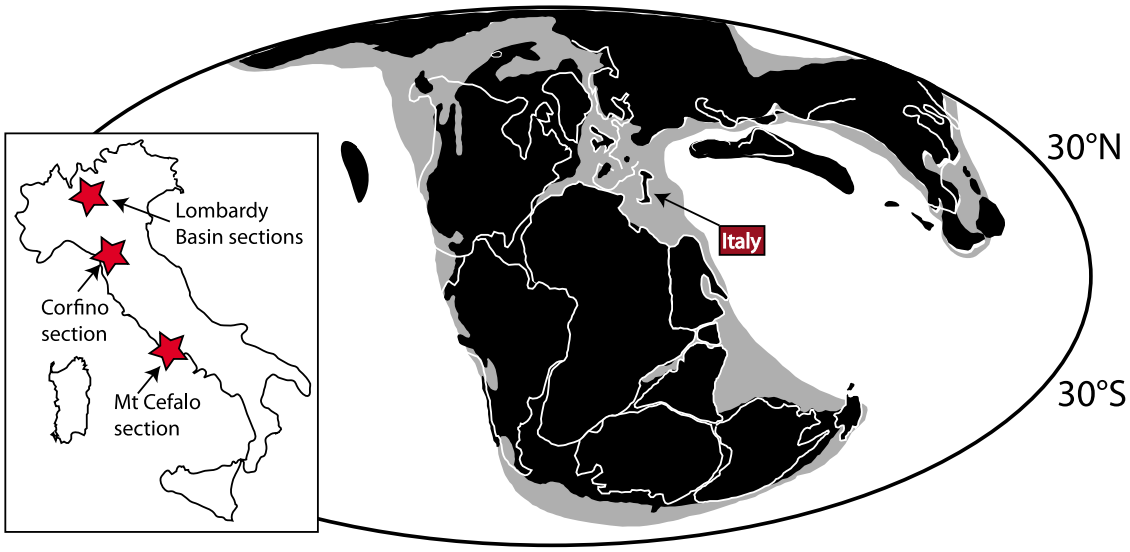

Figure 1. Paleogeographic map of the Early Jurassic world (C. Scotese, PALEOMAP website, 2002, http://www.scotese.com/) [*Golonka*, 2007]. The section locations are as follows: The Val Adrara section is exposed along the road going north from the village of Adrara San Rocco, approximately 1 km from the village at 45°43′29.33″N 9°57′32.29″E. The Pozzo Glaciale section is exposed along the old road on the western shore of Lago d'Iseo approximately 3 km east of the village of Predore at 45°41′5.99″N 10°2′56.83″E. The Italcementi active section is exposed on the southwest facing slope of Mt. Albenza approximately 1 km south of the village of Valcava at 45°46′33.83″N 9°31′9.91″E. The Italcementi Inactive is less than 1 km from the active section at 45°46′35.48″N 9°30′27.09″E. The Corfino section is exposed in the Il Fiume gorge about 2 km northwest of the village of Corfino at approximately 41°11′12.72″N 10°23′46.78″E. The Mt. Cefalo section is exposed on the ESE facing spur of Mt. Cefalo, approximately 6 km north of the village of Gaeta at approximately 41°15′32.05″N 13°32′10.50″E.

[6] The sections investigated in this study (Figure 1) belong to two of these Upper Triassic and Lower Jurassic paleogeographic domains. The sections from the southern Alps (Italcementi Active, Italcementi Inactive, Val Adrara, and Pozzo Glaciale) belonged to the Lombardy Basin and were situated on a gently dipping ramp in a proximal position to the European continent. The sections from the central and southern Apennines (Corfino and Mt. Cefalo) were part of a widespread shallow carbonate platform that is now preserved in central and southern Italy.

2.1. Lombardy Basin Sections

[7] Lithologically, the Triassic portion of the studied sections is represented by the highly fossiliferous Zu limestone. The lower part of the Zu limestone consists of laminated calcareous mudstones with thin shale intercalations that grade into coral-bearing, bioclastic, oncoidal wackestones and packstones. The rocks contain a diverse Triassic assemblage of benthic foraminifera (*Triasina hantkeni*, *Gandinella falsofriedli*, *Aulotortus sinuosus*, *Auloconus permodiscoides*, *Austrocolomia* sp., *Ammobaculites* sp., *Planiinvoluta* sp., and *Nodosariidae* [*Lakew*, 1990; *Galli et al.*, 2007]), bivalves, gastropods, echinoderms, Dasyclad algae, and corals (*Retiophyllia*) [*Lakew*, 1990, 1994]. Carbonate mud was transported from the adjacent platforms, and accumulated in very fine, (millimeter-thick) normally graded laminae (Figure 2a). The coral-bearing limestones are laterally discontinuous and prograde over adjacent mudstone and wackestone beds (Figure 2b).

[8] The Triassic fauna abruptly disappears at the base of the Malanotte Formation, coincident with a meter-thick, carbonate-poor, silty-marly interval (Figure 2d) in the Italcementi Active section, or condensation related iron oxide stained hardground (Figure 2e). The silty-marly horizon, and its correlatives elsewhere, have been interpreted to reflect transgression [*Galli et al.*, 2005], an acidification event [*Hautmann et al.*, 2008], or an influx of volcanic material from CAMP eruptions [*Pálfy and Zajzon*, 2012]. In the Italcementi Active section the silty-marly interval is overlain by a graded bioclastic bed containing coated grains, echinoderms, and foraminifera. In the adjacent Italcementi Inactive section this interval is overlain by a few cm of wackestones containing thin-shelled bivalves. The slumped, thin-bedded mudstones with shale intercalations of the lower Malanotte Formation begin above the silty-marly interval (Figure 2f) [*Galli et al.*, 2005, 2007]. The Malanotte Formation shows a

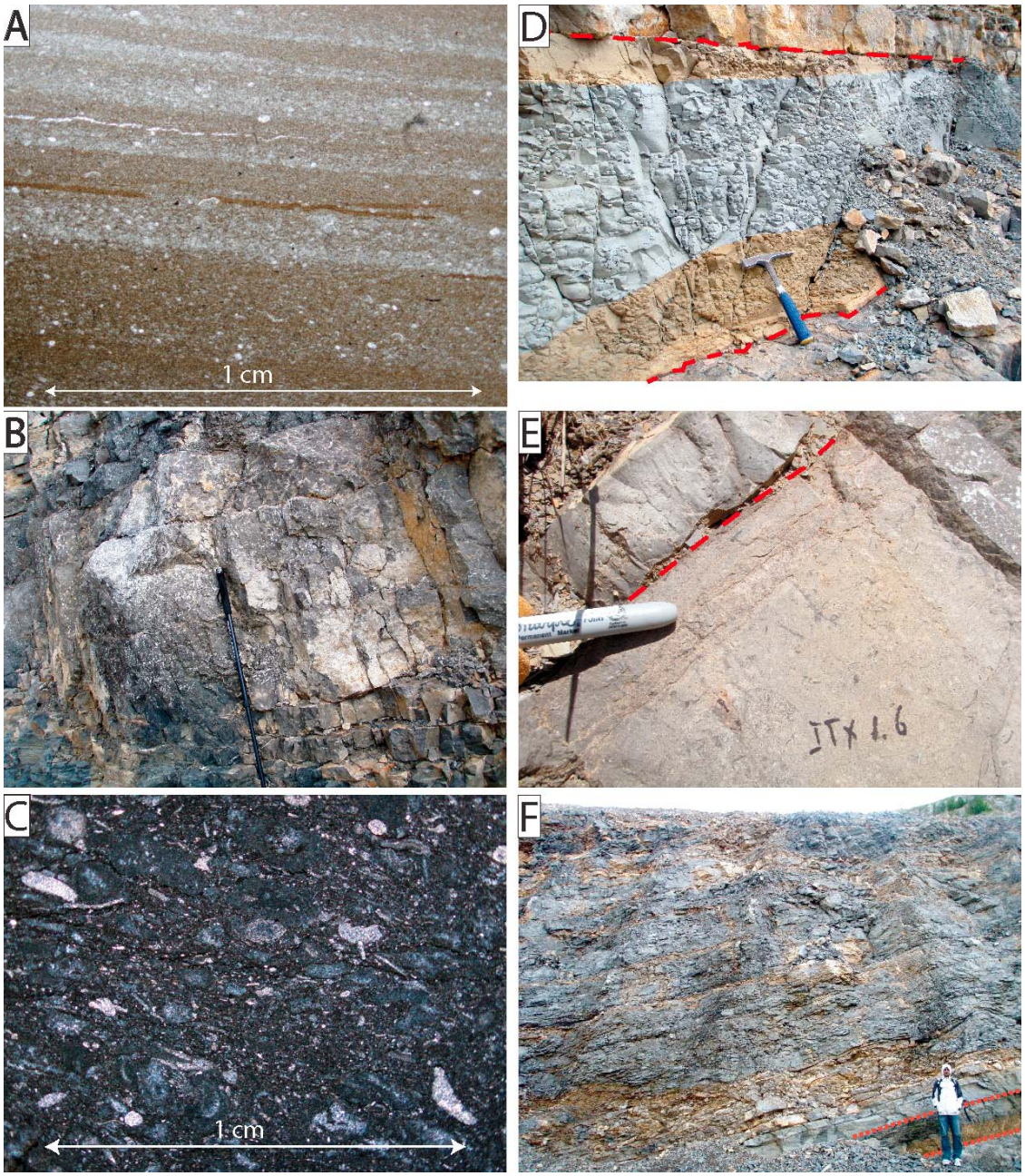

Figure 2. Sedimentary facies of the Lombardy Basin, in stratigraphic order. (a) Upper Triassic outer ramp facies exemplified by laminated thin-bedded mudstone showing normal grading. Thin section from the lower Zu limestone, Italcementi Active section 26.9 m 10×. (b) Coral biohoerm facies in the upper Zu limestone. Note progradation over adjacent mudstones (Italcementi Active section, base of Lower corals). (c) Open marine conditions indicated by abundant echinoderm fragments (top of Zu limestone, Italcementi Active 45.3 m 10×. (d) Silty - marly interval at the top of the Zu limestone, coincident with the disappearance of the Triassic biota, Italcementi Active section. Red stippled lines denote limits of the marl bed. Color variation within is likely due to variations in oxidation of iron minerals. Possible interpretations of marl origin are a marine transgression, a reduction in carbonate production, or an influx of clastic material. (e) Contact between the Zu and Malanotte formations in the Italcementi Inactive section. Here marl is replaced by an iron stained hardground (red stippled line). (f) Transition to deeper water lower Malanotte formation consisting of thin-bedded mudstones. Note obliteration of bedding in lower part by slumping. Marl bed indicated with red stippled lines.

Figure 3. Sedimentary facies from the Lombardy Basin, continued. (a) Bedforms in the upper part of the Malanotte formation indicative of shallowing from the lower Malanotte Formation. (b) Continued shallowing indicated by progradation of oolitic sands at the contact of the Malanotte and Albenza formations. (c) Peak restriction indicated by evaporite pseudomorphs, coincident with the peak of P2. Base of the Pozzo Glaciale section. (d) Return of normal marine conditions, indicated by fossil debris at the base of the Sedrina limestone at the Pozzo Glaciale section, concurrent with the decline of the positive excursion P2. (e) Shallowing in the Pozzo Glaciale section as indicated by oncolitic packstone and (f) crossbedded grainstones in the Sedrina limestone. (g) Chert nodules of the Moltrasio formation, and final deepening of the basin.

progressive increase in grain abundance, a decrease in shale abundance, and increased occurrence of bedforms, such as hummocky cross stratification, upsection (Figure 3a), suggesting a shallowing of relative water depth from a maximum at its base. Based on palynological data (disappearance of *Rhaetipollis germanicus*, and an acme of *Kraeuselisporites reissingeri* associated with other diagnostic Hettangian pollens), the Malanotte Formation has been assigned a Hettangian age [*Jadoul and*

Galli, 2008]. Conodont biostratigraphy and magnetostratigraphy of the Zu and Malanotte formations are consistent with this age assignment [*Muttoni et al.*, 2010].

[9] The contact of the Malanotte Formation with the base of the overlying Albenza Formation is sharp. The base of the Albenza is characterized by oolitic grainstones with dune cross-beds dipping to the NE, which are interpreted as prograding submarine dunes [*Jadoul and Galli*, 2008] (Figure 3b). The Albenza Formation is composed of cross-bedded oolitic, oncolitic and peloidal grainstones, dolmicrites with dissolution pores, and discrete bodies of fabric destructive dolomite. At the base of the Pozzo Glaciale section, some cross-bedded oolitic grainstones with evaporite pseudomorphs occur (Figure 3c). The amount of dolomitization generally decreases upsection. This pattern is especially apparent in the Pozzo Glaciale section. Based on the assemblage of bivalves and gastropods, *Gaetani* [1970] ascribes an Early Hettangian age to this interval (Cenozona 1).

[10] A prominent bed containing coral, echinoderm, and molluscan debris (Figure 3d) occurs at the Albenza-Sedrina contact, where a possible deepening is suggested by a decrease in bed thickness. This bed is also known as the *Chlamys* horizon or the "Grenzbivalvenbank". The fossils found in this interval, and farther up within the Sedrina limestone, indicate an upper Hettangian age (*S. angulata* ammonite zone) for the Sedrina limestone [*Kronecker*, 1910; *Ronchetti and Brena*, 1953; *Gaetani*, 1970; *McRoberts*, 1994; *Jadoul and Galli*, 2008].

[11] The Sedrina limestone shows two facies, representative of two different environments: in the Val Adrara section it is characterized by high mud content (mudstones, wackestones), chert nodules, sponge spicules (which presumably are the source for the chert nodules), and monotonous thin to medium bedding with few bedforms. It is interpreted to have been deposited on a ramp below storm wave base [*McRoberts*, 1994]. In contrast, in the Pozzo Glaciale section the Sedrina limestone is mostly composed of peloidal, oncolitic, and oolitic packstones and grainstones, which are frequently cross-bedded, and chert is absent (Figures 3e and 3f). This facies of the Sedrina limestone is interpreted to have been deposited on a shallowly dipping, frequently wave agitated shelf. It is extremely similar to the Albenza Formation, so much so that in the past they were grouped together into the Corna Formation [*Gaetani*, 1970].

[12] The uppermost formation that we sampled is the Moltrasio Formation, which is composed of thin-bedded limestones with abundant chert (Figure 3g), interpreted as deposited in an outer ramp environment. The Moltrasio Formation has a widespread distribution and a uniform appearance in the Bergamassic Alps, and is interpreted to represent the final drowning of the platform. An upper Hettangian or Sinermurian age has been ascribed to it (Cenozona 3 of *Gaetani* [1970]).

[13] We infer the following relative sea level history from the succession of facies: a shallowing trend from the base of the Zu limestone to the contact with the Malanotte Formation, a rapid deepening around the base of the Malanotte Formation, a progressive shallowing to the middle of the Albenza Formation, and a slight deepening to the Albenza-Sedrina contact. In the Val Adrara section, the deepening trend continues throughout the entire Sedrina Formation until the contact with the Moltrasio Formation, whereas in the Pozzo Glaciale section the shallow environment seen in the Albenza Formation returns until the contact with the Moltrasio Formation. A final, basin-wide transgression establishes the deeper Moltrasio Formation in both sections.

2.2. Corfino Section

[14] At the Corfino section inside the Il Fiume gorge, the Calcare a *Rhaetavicula contorta* consists of medium- to thin-bedded skeletal wackestones and packstones and variably thicker beds of carbonate mudstone. The micro- and macrofauna in the uppermost part of the Calcare a *Rhaetavicula contorta* confirms a Rhaetian age of this unit and is composed of small gastropods, various bivalves including *Rhaetavicula contorta*, and benthic forminifera including *Agathammina passerii*, *Gandinella apenninica* and *Glomospirella rosetta* [*Fazzuoli et al.*, 1988; *Bice et al.*, 1992].

[15] The overlying Calcare Massiccio is composed of thick-bedded to massive carbonate mudstone that has been recrystallized and dolomitized in places. At several intervals, peloids, degraded ooids, and rare bioclastic fragments occur. Fossils are exceedingly rare in the Calcare Massiccio and largely absent in the lower portion of the unit. At Corfino, the base of the Calcare Massiccio has been taken to represent the base of the Hettengian [*Fazzuoli*, 1974; *Bice et al.*, 1992]. Recently, however, *Fazzuoli and Orti* [2006, 2009] reported the benthic foraminifers *Gandinella apenninica* and *Aulotortus sinuosis*

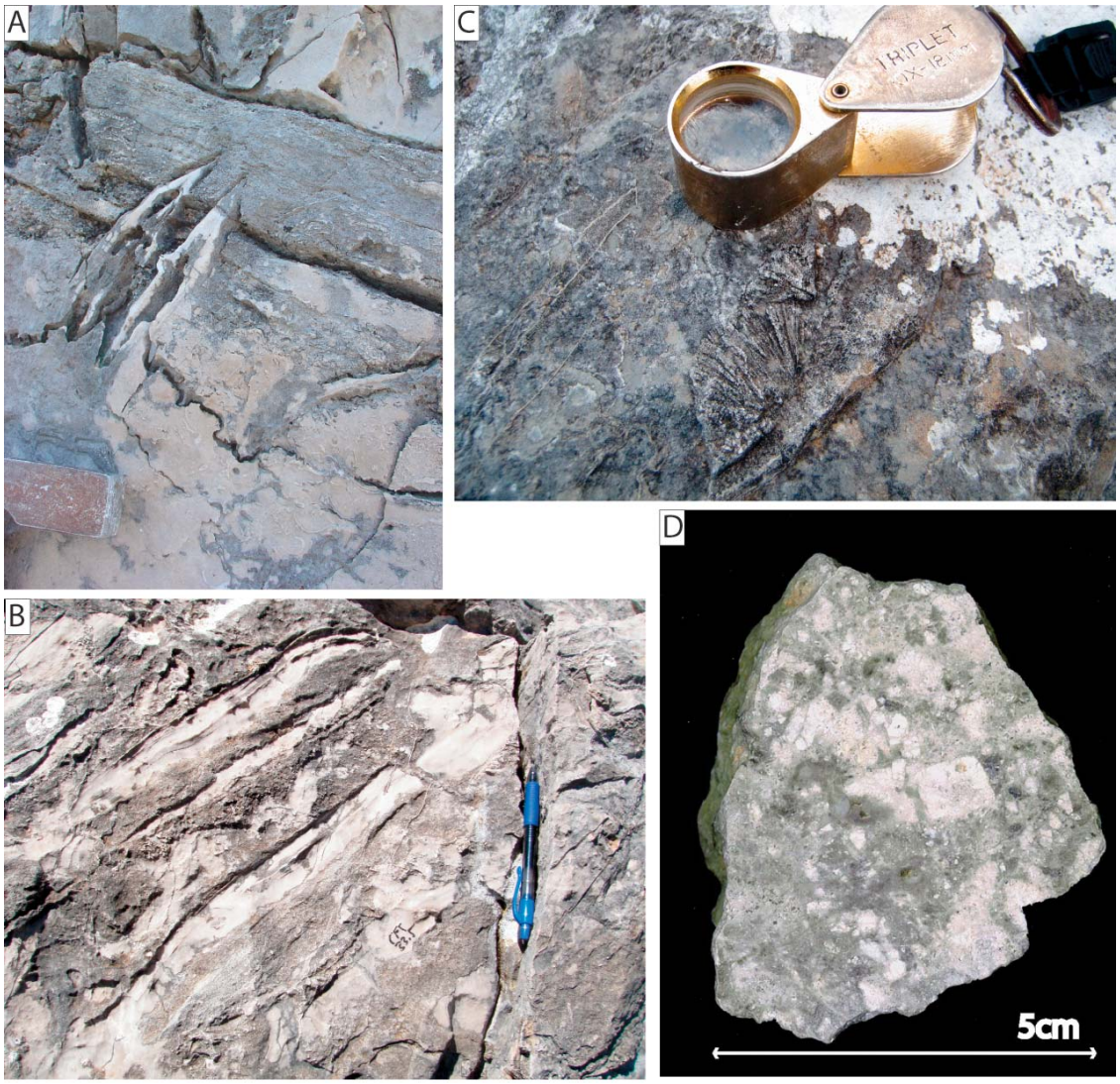

Figure 4. Peritidal limestones of the Mt. Cefalo section (southern Apennines). (a) Typical peritidal facies showing a Megalodont bivalve overlain by fenestral boundstones. (b) Teepee structure in the interval containing the positive excursion (P2). (c) Aragonite crystal fans from the same interval. (d) Polished handsample from the caliche bed in which a negative δ^{13}C excursion (N1) occurs, concurrent with the reduction in the abundance and diversity of the biota, and above which the large positive (P2) excursion begins.

approximately 30 m above the base of the formation. However, these specimens are poorly preserved, hence additional verification is warranted before their presence is conclusively established.

2.3. Mt. Cefalo Section

[16] The predominant facies in both the Upper Triassic and Lower Jurassic of Mt. Cefalo is very pure limestone with no shales. Its more southerly present-day location, approximately 500 kilometers south of the Lombardy Basin, is consistent with the carbonate platform being farther from the source of clastics to the north (Figure 1). The limestones show alternating peritidal facies, with recurring, meter-scale peloidal and oolitic grainstones topped by fenestral boundstones. The Triassic portion contains a rich biota of benthic foraminifera (*Triassina hantkeni* and other Triassic species), the Dasyclad alga *Gryphoporella curvata*, and Megalodont bivalves (Figure 4a) [*Chiocchini et al.*, 1994; *Mancinelli et al.*, 2005; *Barattolo and Romano*, 2005]. Fossils are abundant, and in some horizons the entire rock volume is composed of the calcareous tests of Dasyclad algae and void-filling cements. The biostratigraphy is based entirely on the shallow benthic biota, and no ammonites have been found. However, the nature of

this assemblage indicates a Triassic age for the lower part of the section [*Mancinelli et al.*, 2005]. The Triassic fossils disappear abruptly, coincident with a poorly exposed, meter-thick caliche horizon (Figure 4b). Above this bed, the peritidal facies show a greater degree of restriction, as evidenced by teepee structures (Figure 4c), crystal fans (Figure 4d), pisolites, and laminated fenestral microbial laminites. The peritidal facies continue with very few fossils, and only towards the upper quarter of the section do the diversity and abundance of the biota increase [*Mancinelli et al.*, 2005]. Benthic foraminifera allow the assignment of an upper Hettangian to lower Sinemurian age to this part of the section [*Mancinelli et al.*, 2005].

3. Methods

[17] We analyzed a total of 853 bulk rock carbonate samples for $\delta^{13}C_{carb}$ and $\delta^{18}O$ at the Institute of Geosciences of Goethe University, Frankfurt. We cut the samples to obtain clean surfaces, and drilled the micritic fraction in each hand sample with a dental drill bit while avoiding cements. Samples were acidified in a Gas Bench II (Thermoquest) connected to a continuous flow inlet system of a MAT 253 mass spectrometer. Each sample was analyzed in duplicates ranging from 50 to 100 μgr. An internal standard, calibrated against NBS18 and NBS19, was run along with the samples [*Fiebig et al.*, 2005]. Internal precision was better than 0.05‰ for $\delta^{13}C_{carb}$ and 0.08‰ for $\delta^{18}O$. A detailed description of the analytical setup and the analytical method itself is given in *Spötl and Vennemann* [2003].

[18] We also analyzed a total of 128 samples for the $\delta^{13}C$ of bulk organic carbon at the Stable Isotope Biogeochemistry Laboratory, Stanford University. We pulverized approximately 3 g of rock from each sample in a cast iron mortar and pestle. We placed the samples in a sonicator, and reacted them with between 50 and 250 mL of 20% hydrochloric acid until we observed no more CO_2 production. Recalcitrant samples (containing dolomite) were left overnight in the sonicator. We centrifuged the samples to pellet the particulates, and decanted the acid. We washed the samples by adding 50 ml of vapor distilled water, then centrifuged and decanted the water. We repeated this step 3 times or until the pH of the solution was equal to that of the ultrapure water. Last, we placed the samples overnight in an oven at 50°C to dry. Percent organic carbon of the acidified residue was determined with a Carlo-Erba NA 1500 elemental analyzer. According to the percent carbon in each sample, we weighed out between 100 and 700 μgr of residue for isotopic analysis. The bulk organic carbon analyses were carried out using a Costech Elemental Analyzer ECS 4010 interfaced with a Thermo Finnigan Delta Plus XL mass spectrometer via a Thermo Finnigan ConFlo III unit. External precision of carbon isotope data is better than 0.1‰, based upon repeated measurements of USGS 40 and an internal lab standard (calibrated against USGS 40 and USGS 41). All $\delta^{13}C$ and $\delta^{18}O$ values reported against the VPDB standard.

[19] We used a LOESS procedure (MATLAB, version R2009a, The MathWorks Inc., Natick, Massachusetts) to fit continuous and smooth curves to each data type, and an optimization procedure to obtain the best fitting curve to the data. The 2σ error bounds were obtained by a bootstrap analysis with 500 repetitions. We subtracted the $\delta^{13}C_{carb}$ and $\delta^{13}C_{org}$ curves to get the difference between them.

[20] We constructed the composite curve for the Lombardy Basin by aligning formation boundaries. We used the Val Adrara extended section as a "skeleton" to which the Italcementi Active and Inactive were tied to via the Zu-Malanotte transition, and the Malanotte-Albenza contact. In the case of the Pozzo Glaciale section, only one tie point was available (the Albenza-Sedrina contact), so we used it as an anchor point, and applied a small (15%) stretch to achieve a best fit of the isotopic curves.

[21] The geochemical data for the studied sections is presented in Figures 5–9 for the Lombardy Basin sections (southern Alps), in Figure 10 for the Corfino section (central Apennines), and in Figure 11 for the Mt. Cefalo section (southern Apennines). Composite curves for the Lombardy Basin sections are given in Figure 12 (all data), Figure 13 (samples for which both $\delta^{13}C_{org}$ and $\delta^{13}{}_{carb}$ exist), and Figure 14 (a focus on $\delta^{13}{}_{carb}$). A comparison with other available extended $\delta^{13}C$ records globally is given in Figure 15. A table containing all the $\delta^{13}C_{carb}$, $\delta^{13}C_{org}$, and $\delta^{18}O$ data is given in the auxiliary material.[1]

4. Results

[22] The key features of the record, in stratigraphic order, are small $\delta^{13}C_{carb}$ fluctuations in the uppermost

[1]Auxiliary materials are available at ftp://ftp.agu.org/apend/gc/2012gc004150.

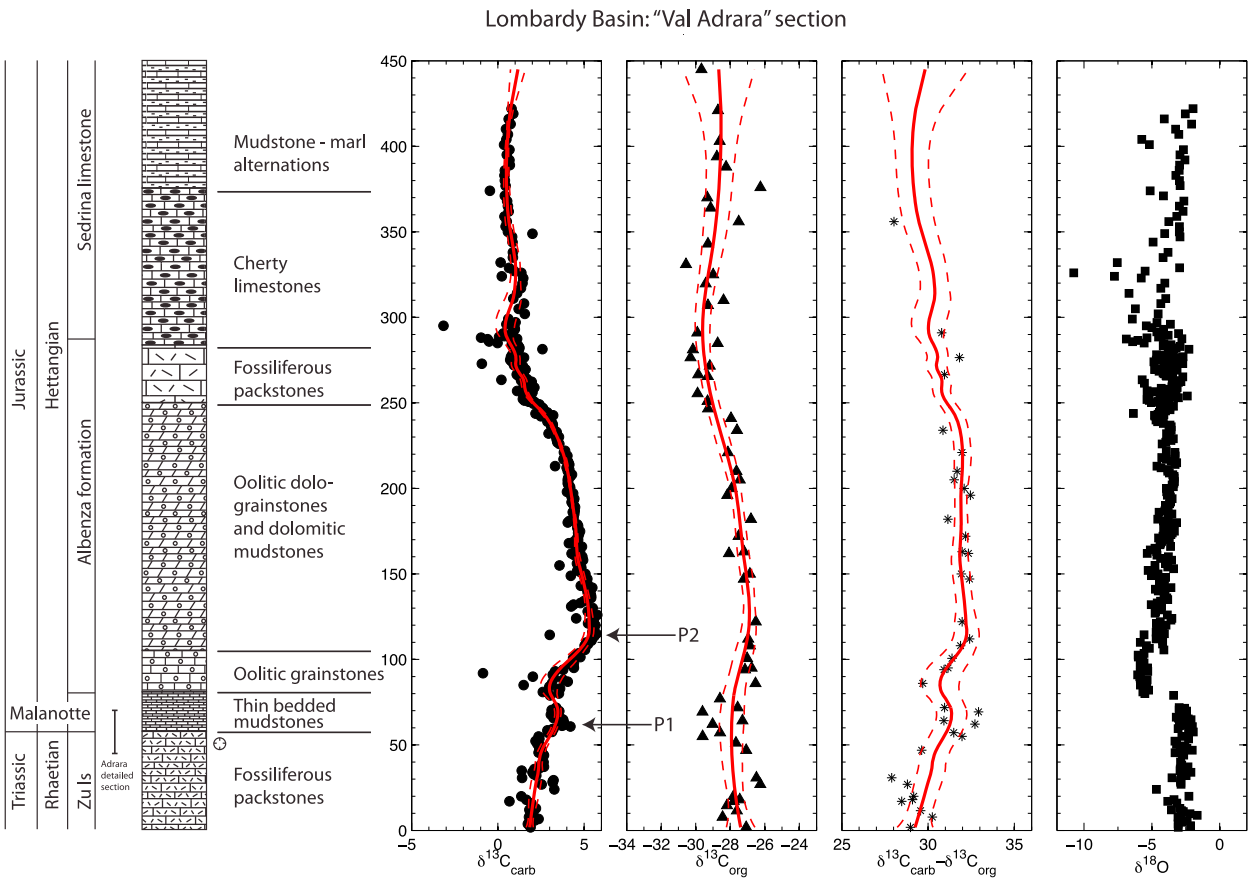

Figure 5. $\delta^{13}C_{carb}$, $\delta^{13}C_{org}$, the difference between them, and $\delta^{18}O_{carb}$, from the Val Adrara section (Lombardy Basin). $\delta^{13}C_{carb}$ and $\delta^{18}O_{carb}$ are from *van de Schootbrugge et al.* [2008]. The red solid line in the two left panels is the average, and the red dashed lines are the confidence intervals (2σ in each direction). The $\delta^{13}C_{carb}$ - $\delta^{13}C_{org}$ panel only shows samples for which both $\delta^{13}C_{carb}$ and $\delta^{13}C_{org}$ were measured. Calculated the average and confidence intervals in the third panel from the left are the difference of the average and confidence intervals of the other two. The occurrence of the isotopic enrichment in both organic and carbonate carbon strongly suggests a primary origin for the signal.

Triassic, a sharp negative excursion in the silty-marly bed above the last occurrence of Triassic fossils (referred to as N1), a small positive excursion (P1), followed by a protracted large positive excursion (P2).

[23] Small scale (<1‰) variation occurs in the $\delta^{13}C_{carb}$ of the uppermost Triassic portion of the Lombardy Basin. These can be seen in the Val Adrara extended (Figure 5) and detailed (Figure 7) sections, and in the Italcementi Active section (Figure 8). Some variation in the average value also occurs in the Mt. Cefalo section (Figure 11), where a substantial thickness (over 100 m) of Triassic section was sampled.

[24] A sharp negative excursion down to −5‰ in $\delta^{13}C_{carb}$ (referred to as N1) occurs in the Val Adrara section (13 m to 15 m at Val Adrara detailed, Figure 7) coincident with the silty-marly horizon, immediately above the last occurrence of the Triassic fauna. This feature is excursion 1 of *Muttoni et al.* [2010] based on the data of *Galli et al.* [2005]. Similarly depleted values occur in the caliche bed above the last Triassic fauna in Mt. Cefalo in the southern Apennines (Figures 11 and 4d).

[25] A small positive excursion of approximately 1.5‰ occurs in $\delta^{13}C_{carb}$ in the lower half of the Malanotte Formation. We refer to this feature as excursion P1, and it corresponds to excursion 2 of *Muttoni et al.* [2010] and its equivalents in the data of *Galli et al.* [2005]. The excursion begins immediately above the silty-marly horizon in the Val Adrara (Figure 7) and Italcementi Active sections (Figure 5), and the iron stained hardground in the Italcementi Inactive section (Figure 9). The initial increase in $\delta^{13}C_{carb}$ is abrupt: in the Italcementi

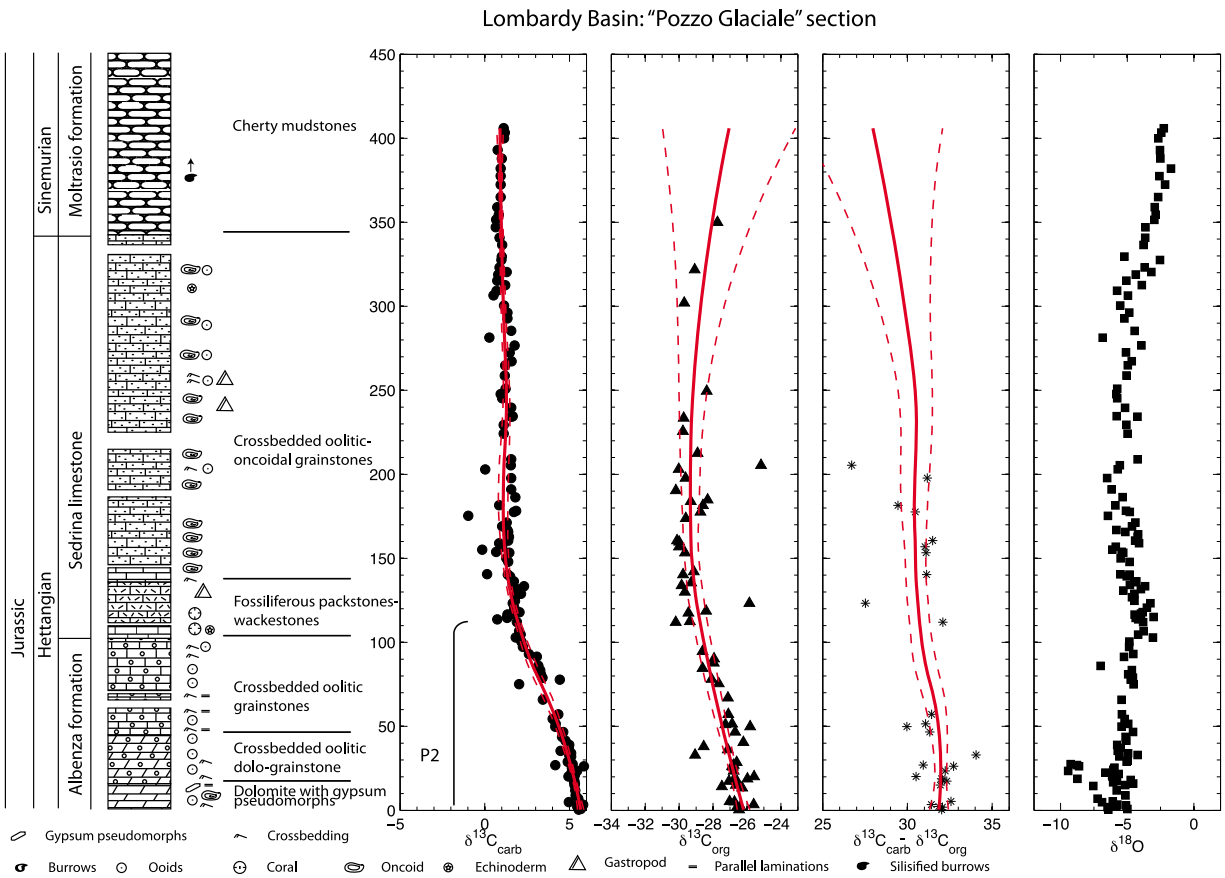

Figure 6. $\delta^{13}C_{carb}$, $\delta^{13}C_{org}$, the difference between them, and $\delta^{18}O_{carb}$ from the Pozzo Glaciale section (Lombardy Basin). Notation as in Figure 5.

Active section it occurs over approximately one meter, in the Italcementi Inactive section it occurs over only a few centimeters. The decline of the P1 excursion is approximately coincident with the transition from the deeper lower half of the Malanotte Formation, to the shallower upper half. An enrichment of similar magnitude occurs in $\delta^{13}C_{carb}$ in a similar stratigraphic position (immediately above the last occurrence of Triassic fossils) in the Corfino section in the central Apennines (Figure 10).

[26] A second protracted excursion in $\delta^{13}C_{carb}$ begins in the upper half of the Malanotte Formation, peaks at a value of about +6‰ near the middle of the Albenza Formation, and then declines to the Albenza-Sedrina contact. This second positive excursion (P2) occurs at the Val Adrara section (Figure 5), at the Pozzo Glaciale section (Figure 6) where only the declining limb is exposed, and at the Italcementi sections (Figures 8 and 9) where only the climbing limb is exposed. The enrichment in $\delta^{13}C_{carb}$ is also broadly reflected in $\delta^{13}C_{org}$. In the Mt. Cefalo section of the southern Apennines (Figure 11), a large positive excursion (up to 5‰) occurs in $\delta^{13}C_{carb}$ immediately above the disappearance of abundant, characteristic, shallow-marine Triassic biota (*Triassina hantkeni* and Megalodont bivalves).

5. Discussion

5.1. Stratigraphic Correlations

5.1.1. The Uppermost Triassic

[27] It is difficult to determine whether the small-scale features that occur in the uppermost Triassic of the studied sections are time correlative. In the Mt. Cefalo section, where a considerable length (≈100 m) of Triassic section was sampled, substantial inter-sample variability obscures any possible underlying trends. Within the Lombardy Basin, the rising limb of a small peak between meters 36 and 44 of the composite record, is the only reproducible

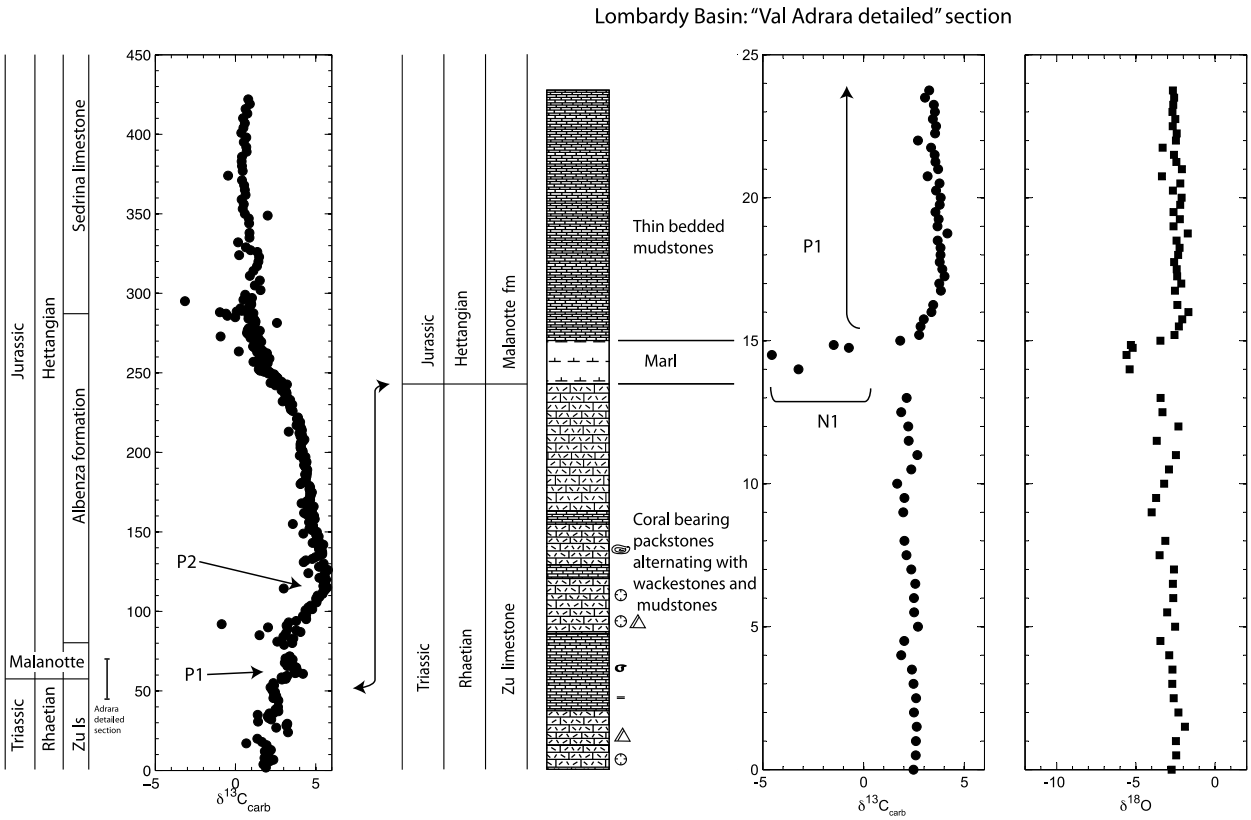

Figure 7. A close up on the boundary interval in the Val Adrara locality. Section is marked as black bar on the left side of the left panel. Correlation with anomalously low δ^{18}O and large lithological change associated with the low carbonate boundary bed suggests a possible diagenetic origin for the N1 excursion.

feature when the different sections are superimposed (Figure 14).

[28] It is similarly difficult to determine how these features relate in time to records from other localities. Small peaks in $\delta^{13}C_{org}$ (1–2‰) occur in the Upper Triassic of Austria [*Kürschner et al.*, 2007], St Audries Bay, UK [*Hesselbo et al.*, 2002], and the Argana Basin in Morocco [*Deenen et al.*, 2010], and have been interpreted as global carbon cycle perturbations resulting from early volatile release events from the CAMP [*Ruhl and Kürschner*, 2011]. The lack of similarity, however, in the δ^{13}C variability that occurs in the Zu limestone within the Lombardy Basin, suggests that the small peaks in the Triassic of the Lombardy Basin are probably local features or, if global in origin, were locally poorly recorded.

5.1.2. The N1 Excursion

[29] A negative excursion in $\delta^{13}C_{org}$ occurs at the extinction horizon in multiple locations worldwide, most notably at the GSSP in Austria [*Ruhl et al.*, 2011]. It is possible that the N1 negative excursion in $\delta^{13}C_{carb}$ within the silty-marly bed correlates with this feature (as *Galli et al.* [2005] suggested), especially since the biostratigraphy suggests such a correlation.

[30] However, several other factors suggest that caution is warranted. First, the negative isotopic values are uniquely associated with a carbonate poor layer, and are never found in carbonate rich limestones (they are absent from Italcementi Inactive, the Corfino section, and other sections reported by *Galli et al.* [2005] that do not contain a boundary marl). Second, the data of *Galli et al.* [2005] show that the organic carbon actually becomes *more enriched* within the boundary marl, in contrast to the carbonate carbon. Third, a correlation with more negative oxygen isotope values strongly hints at a possible diagenetic origin (Figure 7). The same can be said for the caliche layer in the Mt. Cefalo section, which we interpret as non-marine in origin with strong meteoric influences. Currently we hypothesize that the $\delta^{13}C_{carb}$ excursion seen in the silty-marly horizon within the Lombardy Basin and

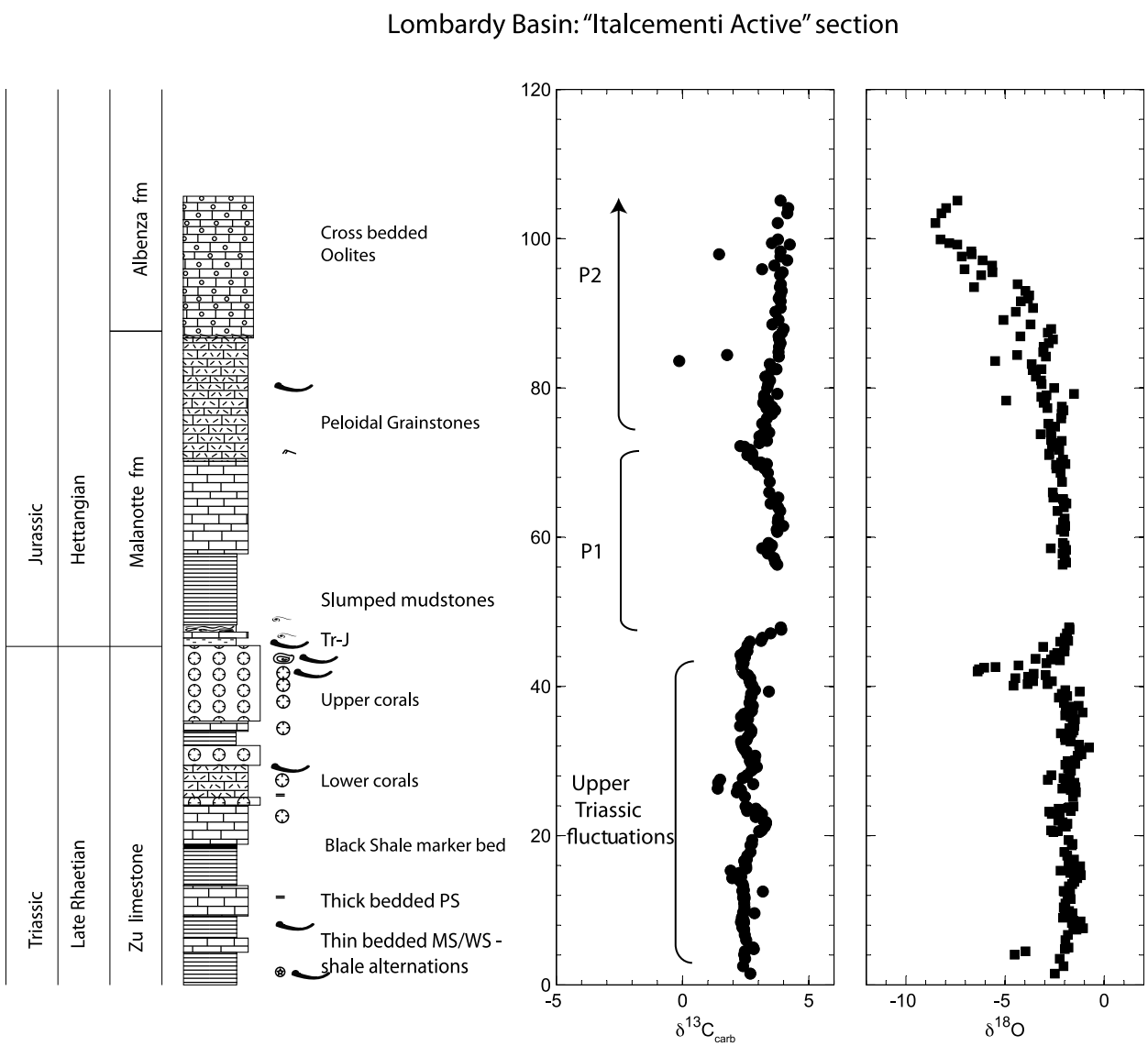

Figure 8. $\delta^{13}C_{carb}$ and $\delta^{18}O_{carb}$ data from the Italcementi Active quarry (Lombardy Basin). Most of the P1 excursion occurs in this section (although some of it is missing due to poor exposure). The rising limb of the P2 excursion is also present.

in the caliche layer at Mt. Cefalo are not features of the global carbon cycle, and most likely are diagenetic in origin.

5.1.3. The P1 Excursion

[31] The P1 excursion is clearly traceable within the Lombardy Basin (Figure 14) [*Galli et al.*, 2005, Figure 3], but the enrichment in $\delta^{13}C_{carb}$ is not reflected in $\delta^{13}C_{org}$. Neither our measurements of $\delta^{13}C_{org}$ at Val Adrara, nor the data of *Galli et al.* [2005] show commensurate enrichment of $\delta^{13}C_{org}$. In contrast, a few relatively ^{13}C-depleted values occur in our data, but these values do not occur in the data of *Galli et al.* [2005], and therefore may be non-representative. Additionally, the increase in $\delta^{13}C_{carb}$ is partially correlated with an increase in $\delta^{18}O_{carb}$ in some sections (Figures 7–9), but not others [*Galli et al.*, 2005, Figure 3] (see also Figure 5). Hence a diagenetic origin is possible.

[32] On the other hand, we note that some carbon cycle scenarios predict a muted response of $\delta^{13}C_{org}$ relative to $\delta^{13}C_{carb}$ (see discussion below); hence this feature might have a primary origin. Perhaps the strongest support for a primary origin and global expression of the P1 excursion, is a similarity with the pattern of $\delta^{13}C_{org}$ that occurs in the Hettangian

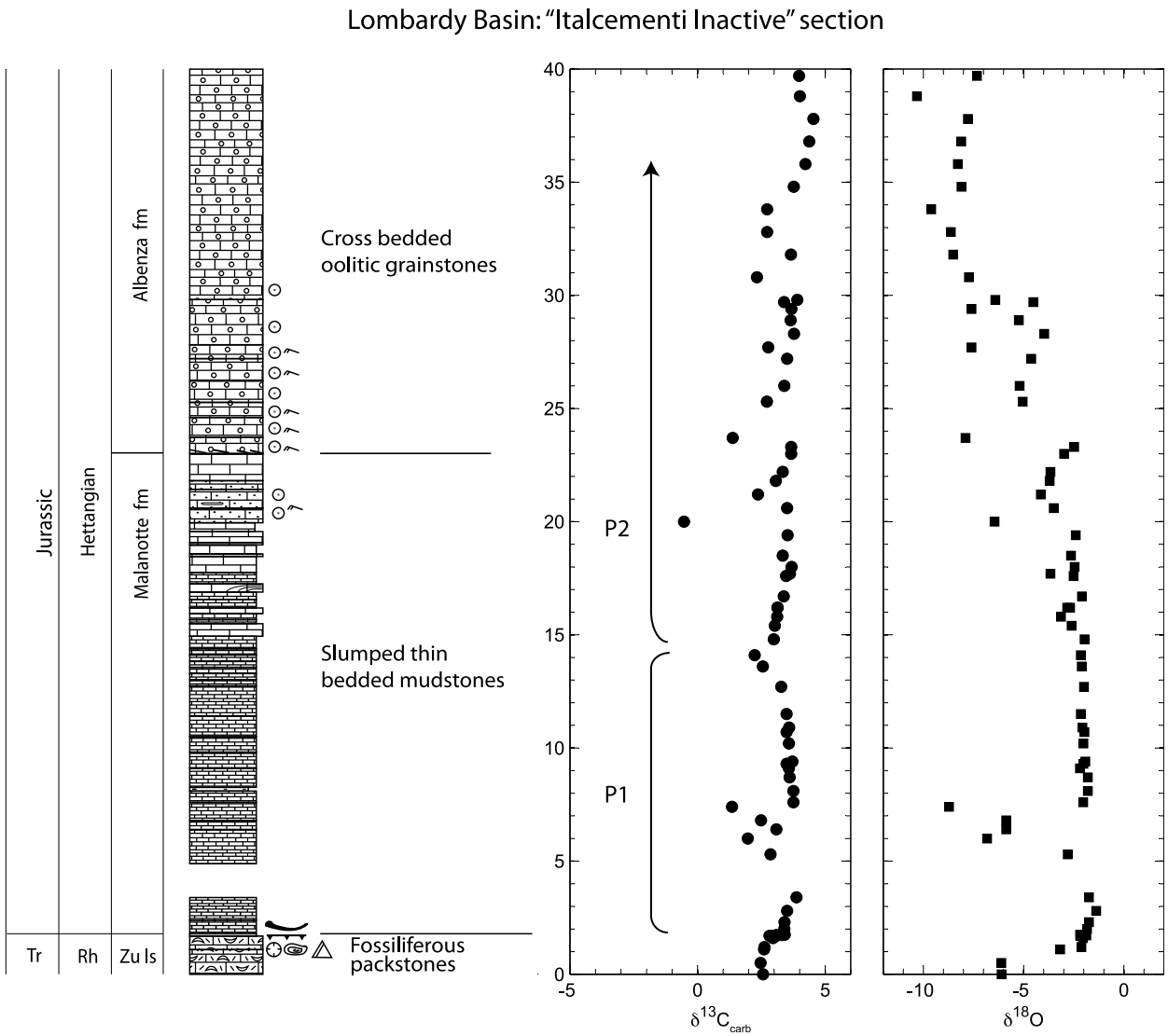

Figure 9. $\delta^{13}C_{carb}$ and $\delta^{18}O_{carb}$ data from the Italcemenit Inactive quarry (Lombardy Basin). The P1 excursion and the rising limb of the P2 excursion occur in this section.

of New York Canyon, Nevada (Figure 15): one small (2‰) positive excursion occurs in the *P. planorbis* ammonite zone in the lower Hettangian (excursion 2 of *Bartolini et al.* [2012]), and another larger positive excursion occurs in the *S. angulata* ammonite zone of the upper Hettangian (excursion 7 of *Bartolini et al.* [2012]). Additional positive excursions in equivalent biostratigraphic positions (near the *P. planorbis* zone) are the small positive $\delta^{18}C_{carb}$ excursion that occurs in and above the Langport member in St. Audrie's Bay [*Korte et al.*, 2009], and its correlative in organic carbon, the small positive excursion between the "initial" and "main" excursions that occur in the $\delta^{13}C_{org}$ of UK and Austria [*Hesselbo et al.*, 2002; *Ruhl et al.*, 2009] (Figure 15).

5.1.4. The P2 Excursion

[33] Based upon magnitude, stratigraphic thickness, and position above the last occurrence of diagnostic Triassic fossils, the P2 excursions of the Lombardy Basin and Mt. Cefalo can be interpreted as time equivalent, with a Hettangian age. A primary origin is strongly suggested by the enrichment in both $\delta^{13}C_{carb}$ and $\delta^{13}C_{org}$ (Section 5.2.1).

[34] Several other records exhibit large positive excursions in $\delta^{13}C_{org}$ in the upper Hettangian. At New York Canyon, Nevada, a positive excursion in $\delta^{13}C_{org}$ occurs within the *S. angulata* ammonite zone (excursion 7 of *Bartolini et al.* [2012]). Similarly, a large positive excursion in $\delta^{13}C_{org}$ occurs

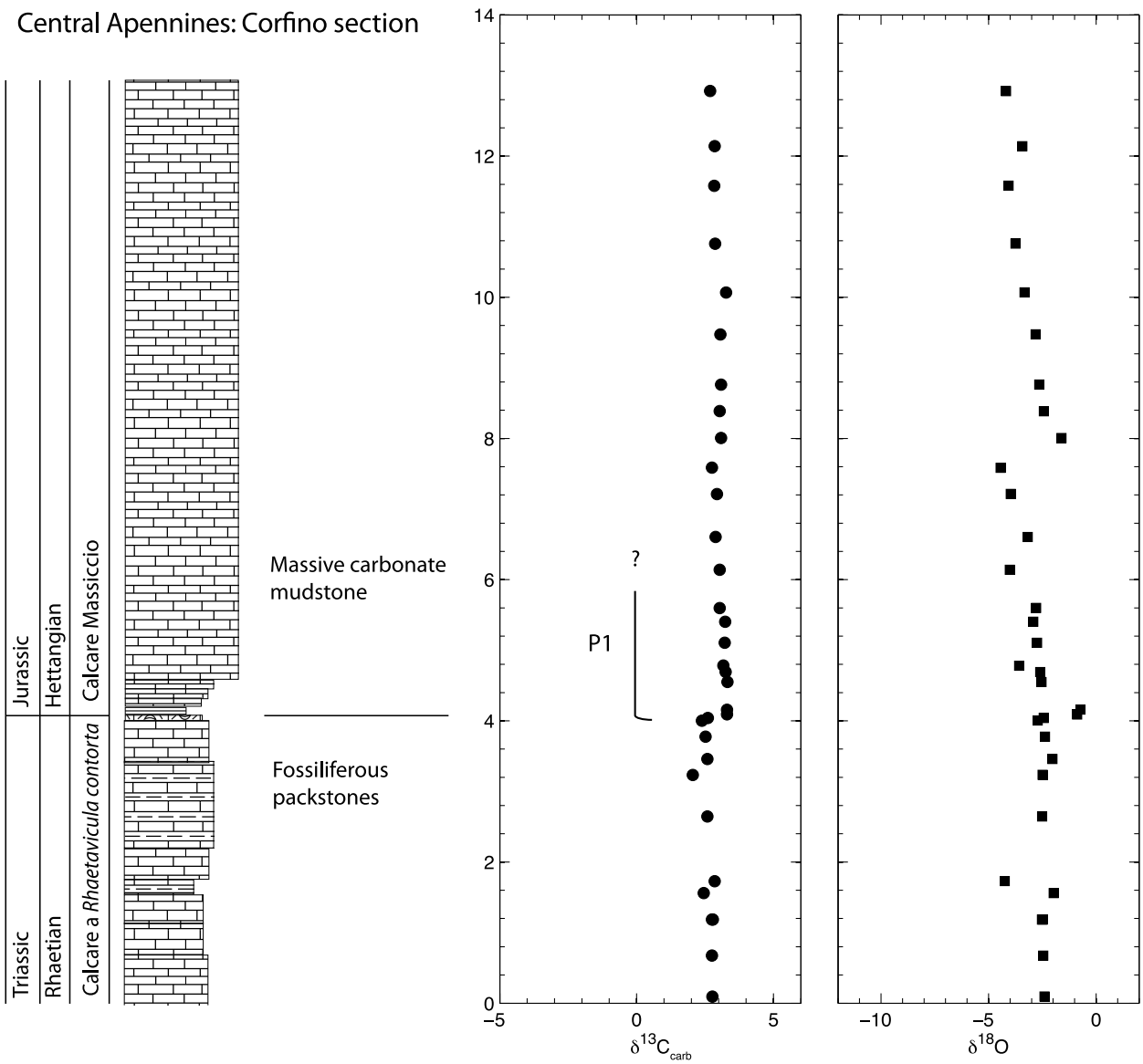

Figure 10. $\delta^{13}C_{carb}$data from the Corfino section, in the central Apennines. We interpret the small $\delta^{13}C_{carb}$ above the last occurrence of Triassic fossils to be correlative with the P1 excursion.

in the Hettangian of Queen Charlotte Island. Originally placed in the lower Hettangian (*A. liassicus* zone), it has been assigned an upper Hettangian age by *Bartolini et al.* [2012] based on a re-interpretation of the data of *Longridge et al.* [2008] and *Tipper et al.* [1991]. Although a large positive excursion in the upper Hettangian has characterized some of the sections studied to date, a major challenge for a global synchronous expression of the P2 excursion comes from the well studied sections in the SW UK [*Hallam*, 1981, 1994; *Hounslow et al.*, 2004; *Hesselbo et al.*, 2004; *van de Schootbrugge et al.*, 2007; *Korte et al.*, 2009; *Ruhl et al.*, 2010a] where no enrichment occurs anywhere in the upper Hettangian.

5.2. Origin of the ^{13}C Enrichment

[35] Typically, variations in the δ^{13}C of carbon with durations much longer than the residence time of carbon in the ocean-atmosphere system (10^3 yrs [*Broecker and Peng*, 1982]), have been interpreted as representing the δ^{13}C of a well mixed reservoir [e.g., *Hayes et al.*, 1999; *Kump and Arthur*, 1999]. The duration of the P2 positive excursion is at least half the Hettangian (≈1 my [*Guex et al.*, 2012]), which is well beyond the residence time of carbon, indicating that the same δ^{13}C pattern should occur in all sections. However, the variability in the observed isotopic trends in different localities (Figure 15), suggest that explanations other than a

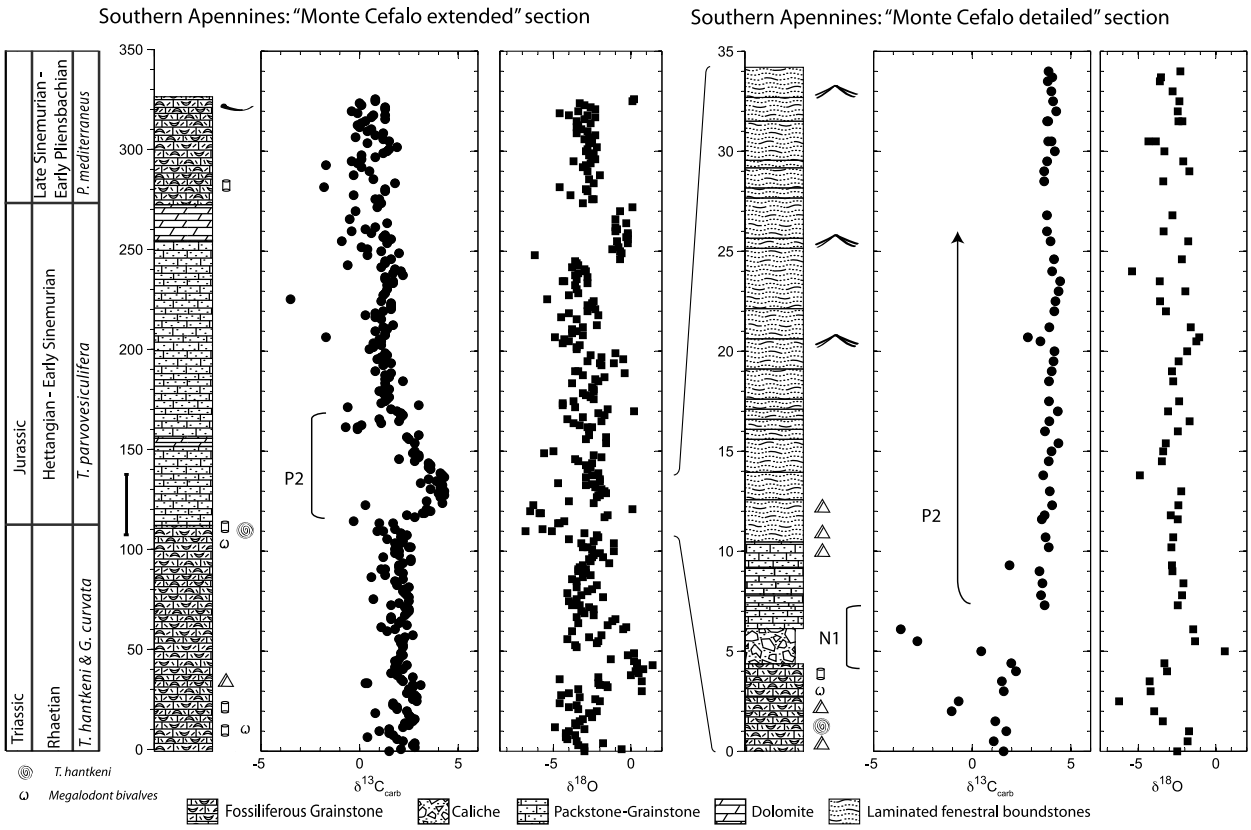

Figure 11. $\delta^{13}C_{carb}$ data from the Mt. Cefalo section (southern Apennines). The section on the right (Mt. Cefalo detailed) is centered around the boundary, and its position in the larger section is marked left of the left log. We interpret the large $\delta^{13}C_{carb}$ increase above the last occurrence of Triassic biota to be correlative with the P2 excursion. The absence of the P1 excursion is taken to be a result of a hiatus at the base of the excursion, which is consistent with the evidence for exposure (caliche bed), and abrupt transition to enriched $\delta^{13}C_{carb}$ values.

shift in the isotopic composition of the combined ocean-atmosphere pool should be explored.

5.2.1. Diagenetic Contribution

[36] A number of arguments suggest that the P2 excursion, at least, is unlikely to be of diagenetic origin. First, no correlation is evident between the $\delta^{13}C_{carb}$ and $\delta^{18}O$ records (Figure 12). Second, the ^{13}C enrichment occurs in both carbonate and organic carbon (Figure 13), and no post-depositional mechanisms are known to be capable of simultaneously enriching the isotopic compositions of both organic and carbonate carbon in sediments [*Knoll et al.*, 1986]. Third, the positive excursion can be traced between sections across the Lombardy Basin for a distance of approximately 40 kilometers (Figure 14), and within individual sections it appears gradual across sharp lithofacies transitions. Finally, it occurs at a similar stratigraphic position (i.e. above the last beds containing a rich and diverse assemblage of Triassic fossils), 500 kilometers away in a region with a different tectonic and diagenetic history.

5.2.2. Local Enrichment

[37] On modern carbonate platforms, restricted (that is, with poor connection to the open ocean) and evaporative conditions are often associated with elevated $\delta^{13}C$ values [*Stiller et al.*, 1985; *Shinn et al.*, 1989; *Gischler et al.*, 2009]. This phenomenon can be due to local organic carbon burial driving the local carbon pool to more enriched values, or kinetic effects associated with CO_2 removal during evaporation [*Zeebe and Wolf-Gladrow*, 2001]. Alternatively, an increase in the $\delta^{13}C$ of the weathering flux or an increase in $\delta^{13}C$ of the incoming particulate organic carbon could drive a local carbon pool to more elevated $\delta^{13}C$ values [*Lloyd*, 1964; *Patterson and Walter*, 1994].

[38] Either way, for a local reservoir to develop its own distinct signature ^{12}C removal must outpace

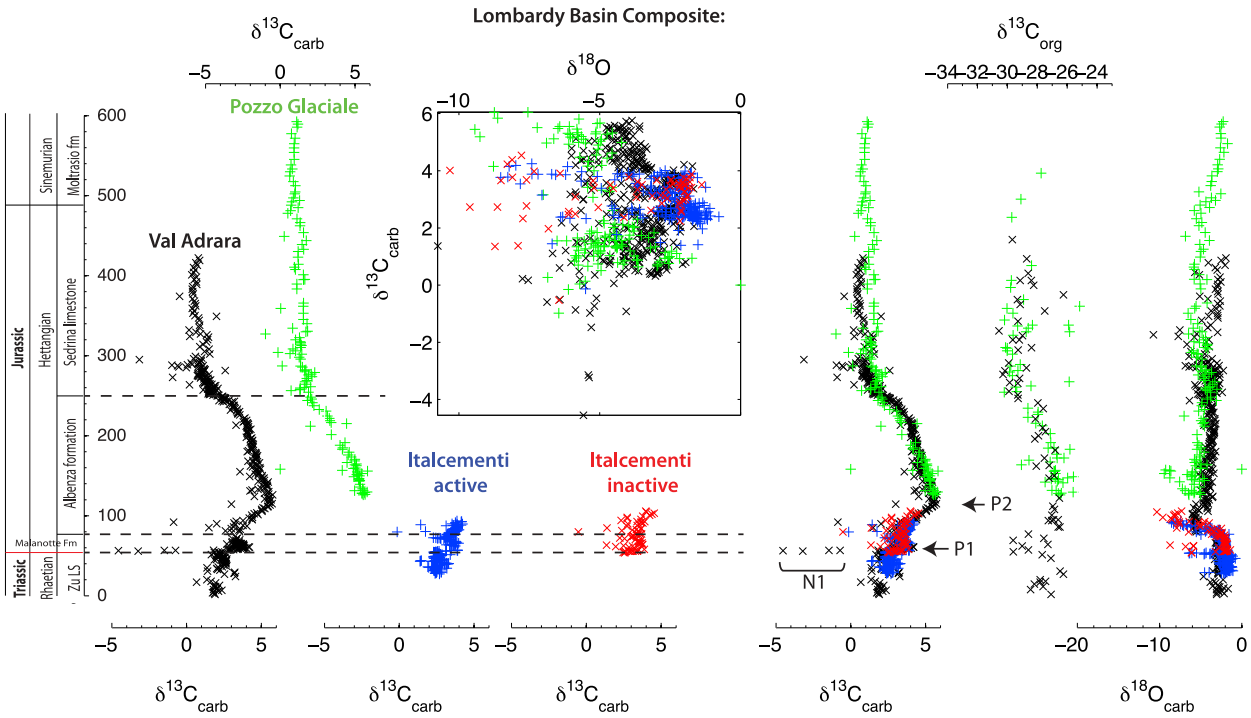

Figure 12. A composite of the Lombardy Basin sections (southern Alps) showing $\delta^{13}C_{carb}$, $\delta^{13}C_{org}$, and $\delta^{18}O$ data. Dashed horizontal lines are lithologic tie points between sections.

the countering effects of mixing with the shallow ocean and carbon exchange via the atmosphere (which would tend to homogenize the $\delta^{13}C$ of a small reservoir with that of the global surface ocean [*Junge et al.*, 1975]). In the geological record, sea level fall or tectonic uplift might conceivably decrease the connection of a local basin to the open ocean, thereby driving up its tendency to develop a distinct signature that is unrepresentative of the global carbon cycle.

[39] Indeed, in the studied sections, the P2 excursion partially correlates with the sedimentary facies. The most positive $\delta^{13}C_{carb}$ values coincide with the most evidence for restriction, such as: dolmicrites in the Albenza Formation in the Val Adrara extended section, cross bedded oolites/peloids with evaporite pseudomorphs in the Albenza Formation in the Pozzo Glaciale section (Figure 3c), and teepees and crystal fans in the Mt. Cefalo section (Figures 4c and 4d). Moreover, the partial correlation with facies observed in the Lombardy Basin sections and in Mt. Cefalo is also shared by the Canadian section where the large positive excursion in $\delta^{13}C_{org}$ corresponds to a transition from mudstones to turbiditic sandstones with abundant woody debris [*Williford et al.*, 2009], suggesting an influx of ^{13}C-enriched terrestrial carbon [*Arthur et al.*, 1985].

[40] A number of observations, however, suggest that the P2 positive excursion is not a *simple* function of facies. First, supratidal sediments, such as those that appear in conjunction with the positive excursion, appear in the Mt. Cefalo section at other levels (Figure 4a), and these are not accompanied by elevated $\delta^{13}C$ values. Second, in the Pozzo Glaciale section, the Sedrina limestone shows equally shallow facies as the underlying Albenza Formation in which the positive excursion occurs (Figure 3f), and it is not accompanied by elevated $\delta^{13}C$ values. In fact, the two formations are so similar, that in the past they were grouped into one shallow marine facies (the Corna Formation [*Gaetani*, 1970]). The return to shallow, restricted conditions in the Sedrina Limestone, after the slight deepening at the Albenza-Sedrina boundary, is not accompanied by another positive excursion, which would be predicted if it were entirely facies dependent. Third, by measuring the $\delta^{13}C_{carb}$ along a depth gradient, we can estimate the contribution of depositional environment to the overall isotope composition of the limestones. The Val Adrara facies of the Sedrina limestone is composed of cherty limestones and lime-marl alternations with few sedimentary structures, and is inferred to have been deposited below storm wave base. The Pozzo Glaciale facies is composed of limestones with

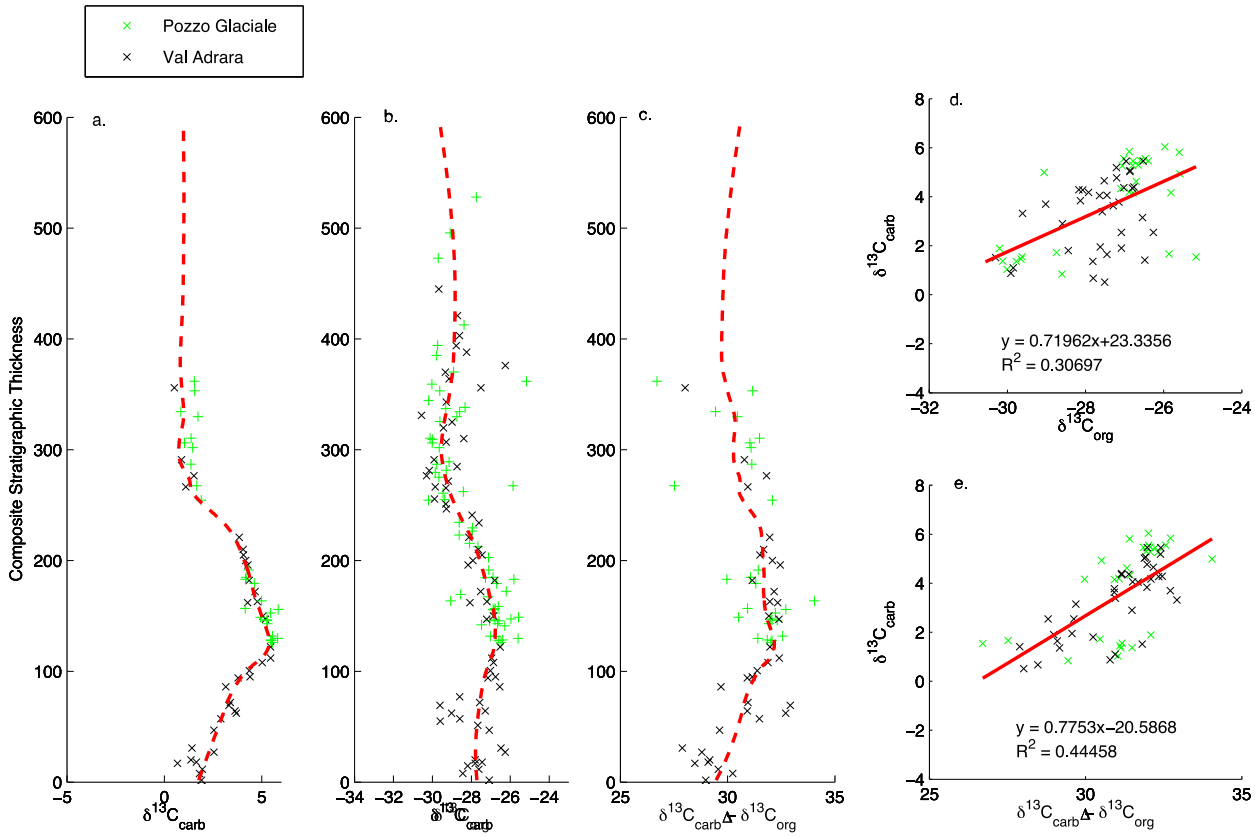

Figure 13. Composite carbonate and organic carbon isotopic data for the Val Adrara and Pozzo Glaciale Sections. In Figure 13a only the $\delta^{13}C_{carb}$ values of points that have *both* organic carbon and carbonate carbon measurements on them are plotted. We have added the average of all available carbonate data to guide the eye (dashed line). Dashed line in Figure 13b is average of the plotted organic carbon data, and dashed line in Figure 13c is the difference between the two.

abundant oncolites that are commonly crossbedded, and is inferred to have been deposited in a shallower environment above wave base. The δ^{13}C difference between them in stratigraphically equivalent horizons (the green and black curves in Figure 12), is only approximately 0.5‰. This observation suggests that if the positive carbon isotope excursions resulted from a local gradient (i.e. the shifting of facies belts with very different isotopic values), this local gradient did not persist into the latest Hettangian and Sinemurian. Consequently, we suggest that the observed correlation between the δ^{13}C value and facies is more likely to be a product of concurrent but independent processes, than a strict δ^{13}C dependence on facies.

5.3. Carbon Cycle Considerations

[41] There are more general reasons, however, to reject the hypothesis that the P2 excursion is simply product of local processes. There are few crustal reservoirs of isotopically enriched carbon, therefore the most likely candidate for driving ^{13}C enrichment is the removal of ^{13}C-depleted organic carbon, which can occur locally or globally. Yet, if local, there is a strong upper limit on the amount of ^{13}C-enriched carbon that can be buried without affecting the average composition of the ocean-atmosphere carbon pool. On timescales much longer than the residence time of carbon, the isotopic composition of the carbon output flux from sedimentation of carbonate ($\delta^{13}C_{carb}$) and organic carbon ($\delta^{13}C_{org}$) must equal the average δ^{13}C of inputs from weathering and volcanism ($\delta^{13}C_{in}$):

$$\delta^{13}C_{in} = f_{org}\delta^{13}C_{org} + (1 - f_{org})\delta^{13}C_{carb}$$

where f_{org} is the fraction of organic carbon burial of the total carbon burial flux. If the burial of locally enriched carbon (with a $\delta^{13}C_{carb}$ and/or $\delta^{13}C_{org}$ larger than that defined by the long term equilibrium) became quantitatively important it would shift the balance so that the average δ^{13}C of the output would become more ^{13}C-enriched than the input. If not countered by burial of less ^{13}C-enriched carbon elsewhere, the result would be accumulation of ^{12}C

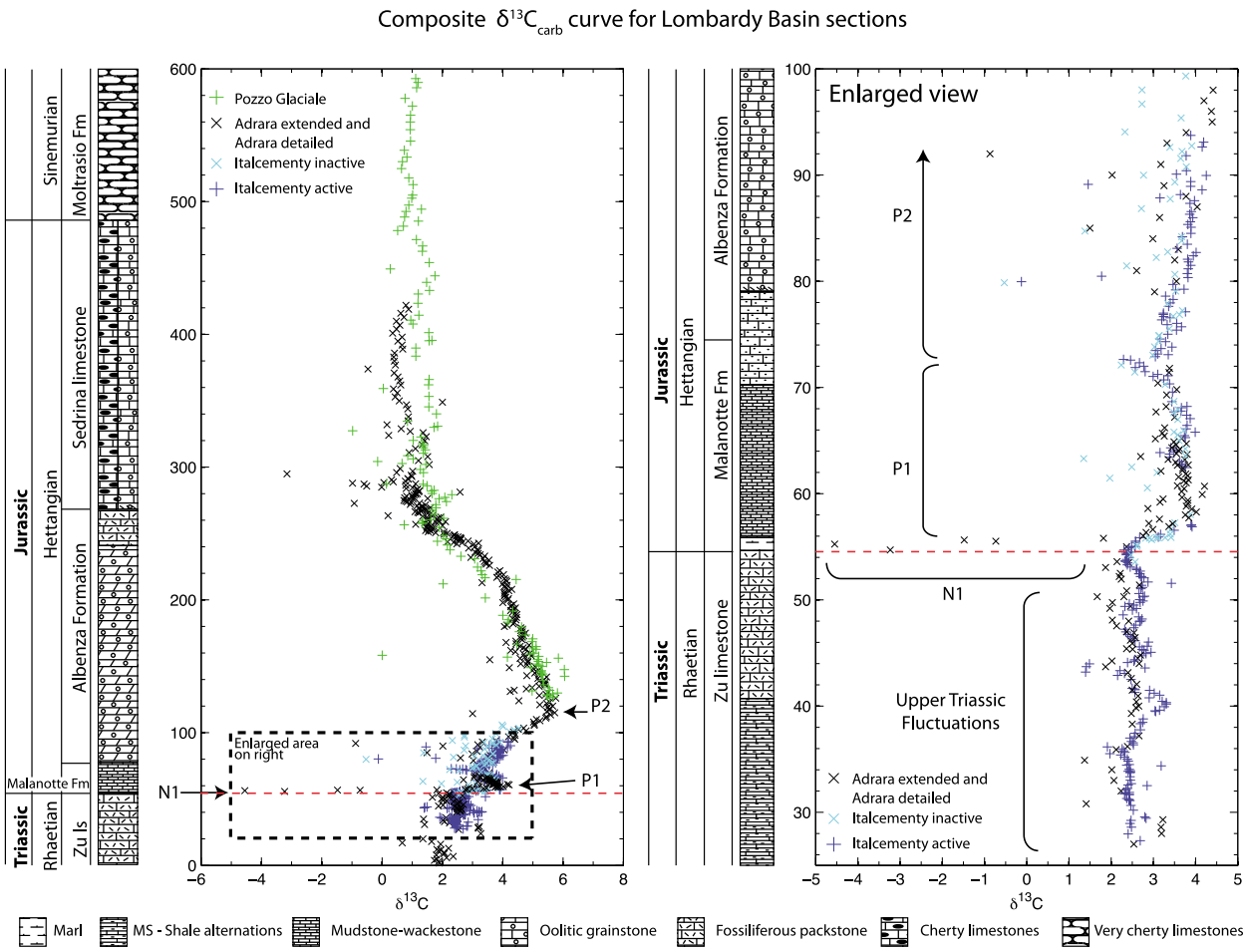

Figure 14. Composite section, and detailed view of the Lombardy Basin $\delta^{13}C_{carb}$ curve. Val Adrara data are from *van de Schootbrugge et al.* [2008]. See Figure 12 for section correlations.

in the ocean until the isotopic mass balance was regained, expressed as negative excursions elsewhere. This is a key point: local deviations from the global curve [e.g., *Swart*, 2008] can only ever be quantitatively unimportant in terms of the overall burial flux, as otherwise they would affect the global isotopic balance in the opposite direction. This limitation on shelf carbonate deposits would be even more stringent in a world without a pelagic carbonate sink, when shelf sedimentation would have constituted an even greater fraction of the overall carbon burial flux, thus having more leverage on the long term isotopic balance.

5.4. $\delta^{13}C_{org}$ and $\delta^{13}C_{carb}$ Decoupling

[42] In addition to the enrichment that occurs in $\delta^{13}C_{carb}$ and $\delta^{13}C_{org}$, a second salient aspect of the P1 and P2 excursion is that the organic carbon and carbonate carbon show different magnitudes of responses. During the P2 positive excursion, the magnitude of change in $\delta^{13}C_{carb}$ is about twice that of $\delta^{13}C_{org}$ (Figures 5, 6, 12, and 13).

[43] When the $\delta^{13}C_{org}$ and $\delta^{13}C_{carb}$ of the sampled sections are plotted against each other (Figure 13d), the slope of the regression line is indicative of the rate of change of $\delta^{13}C_{org}$ as a function of the change in $\delta^{13}C_{carb}$. A slope of one would have resulted if for every unit increase in $\delta^{13}C_{carb}$, $\delta^{13}C_{org}$ increased by the same amount. The smaller enrichment that occurs in $\delta^{13}C_{org}$ relative to the stratigraphically equivalent $\delta^{13}C_{carb}$ yields a slope that is smaller than one.

[44] If one assumes that the isotopic enrichment in the limestones is representative of the $\delta^{13}C$ of dissolved inorganic carbon in the seawater from which the limestones were deposited, then there are only a few mechanisms by which the $\delta^{13}C$ of TOC might show a smaller magnitude of enrichment.

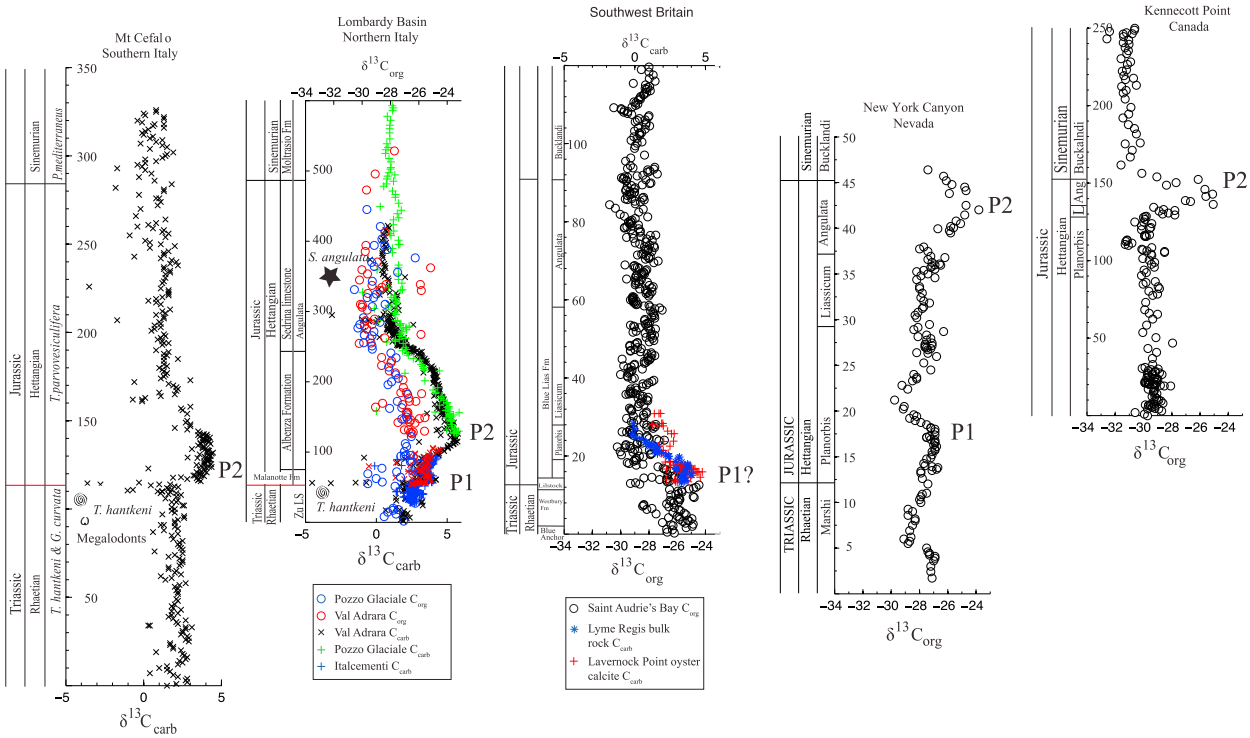

Figure 15. Comparison of data from this study with currently available extended $\delta^{13}C_{org}$ records spanning the uppermost Triassic and lowermost Jurassic. As this figure highlights, currently there is difficulty in reconciling the chemostratigraphy and biostratigraphy. The data are plotted on a linear depth scale with the age estimates marked to the left of each record, and potential correlations of the two positive excursion (P1 and P2), plotted to the right of the data. Hollow points denote organic carbon data, all others carbonate carbon. Red line is extinction horizon. Data from the Queen Charlotte Islands, Canada [*Williford et al.*, 2007], Southwest Britain [*Hesselbo et al.*, 2002, 2004; *Ruhl et al.*, 2010a; *Korte et al.*, 2009], and Nevada, USA [*Bartolini et al.*, 2012].

[45] One end-member that can explain the decoupled response of the $\delta^{13}C_{org}$ and $\delta^{13}C_{carb}$ is that locally produced organic carbon comprises only part of the sampled TOC [*Johnston et al.*, 2012]. The degree of muting depends on the proportion of recycled organic carbon ($f_{org}^{recycled}$): if there is none, the magnitude of the positive excursion will be the same in both $\delta^{13}C_{org}$ and $\delta^{13}C_{carb}$, and when $f_{org}^{recycled} = 1$ the organic carbon record will exhibit no trend, and reflect only the distribution of isotopic compositions of the recycled C_{org}. We can estimate the amount and isotopic composition of the recycled organic carbon needed to explain the difference between $\delta^{13}C_{carb}$ and $\delta^{13}C_{org}$ (ϵ_{TOC}^{total}) by fitting a mixing model to data from northern Italy. We assume the mixing of two end-members: one is the locally produced organic carbon with a $\delta^{13}C_{org}$ that is equal to the $\delta^{13}C_{carb}$ minus a constant fractionation factor ($\epsilon_{TOC}^{primary}$), which is taken to be the value of the difference between the two records following the end of the perturbation (31‰), and the other end-member is the recycled organic matter with an unknown $\delta^{13}C_{org}$. The model is given by:

$$\epsilon_{TOC}^{total} = f_{org}^{recycled} \times \delta^{13}C_{org}^{recycled} + \left(1 - f_{org}^{recycled}\right) \times \left(\delta^{13}C_{carb} - \epsilon_{TOC}^{primary}\right)$$

We use multiple linear regression (MATLAB, version R2009a, The MathWorks Inc., Natick, Massachusetts) to obtain the most likely values for $f_{org}^{recycled}$ and $\delta^{13}C_{org}^{recycled}$. For the Val Adrara section a contribution of recycled carbon comprising 0.6 ± 0.15 of the total with an isotopic composition of -28.3 ± 0.4‰, and for the Pozzo Glaciale section a contribution of 0.5 ± 0.2 with a $\delta^{13}C_{org}$ of -28.5 ± 0.7‰, are sufficient to explain the muted $\delta^{13}C$ response of the organic carbon.

[46] The other end-member is that the fraction of extra-basinal carbon ($f_{org}^{external}$) was low, and the increase in the magnitude of the difference between $\delta^{13}C$ of the limestones and $\delta^{13}C$ of the measured

TOC is representative of an increase in the magnitude of the difference between the precipitating limestones and the locally produced organic carbon at the time of the excursion ($\epsilon_{TOC}^{primary}$). The isotopic difference between the limestones and the contemporaneously produced organic matter ($\epsilon_{TOC}^{primary}$) is influenced by several factors [*Hayes et al.*, 1999]: an approximately 8‰ fractionation between DIC and carbonates which is strongly temperature dependent [*Deuser*, 1970], a fractionation associated with the fixation of CO_2 which is dependent on algal growth rates [*Laws et al.*, 1995; *Bidigare et al.*, 1997], algal morphology [*Popp et al.*, 1998], and $CO_{2,aq}$ concentrations [*Hollander and McKenzie*, 1991; *Freeman and Hayes*, 1992], and lastly, a component from secondary processes such as heterotrophic respiration [*Hayes et al.*, 1989]. The contribution of each of these effects to the overall bulk organic carbon can be determined by measuring individual microfossils [*Kaufman and Xiao*, 2003] or biomarkers [*Hayes et al.*, 1989], and is beyond the scope of this paper.

[47] We hypothesize that the most likely explanation for the muted response of the organic carbon involves contributions from both recycled inert carbon and an increase in fractionation in response to a possible increase in $pCO_{2,aq}$, a decrease in temperature, decreased algal growth rates, or a decrease in secondary reworking.

6. Conclusions

[48] In aggregate, available data indicate an ongoing perturbation of the global carbon cycle during Hettangian time. In particular, a protracted interval of ^{13}C enrichment occurs in records from both carbonate and organic carbon from most Hettangian sections, spanning multiple ocean basins. Because no diagenetic mechanisms are known to alter both carbonate and organic carbon in the same direction at the same time, the demonstration of covariation of $\delta^{13}C_{carb}$ and $\delta^{13}C_{org}$ in stratigraphic sections from the Lombardy Basin provides strong confirmation of a primary origin for this feature.

[49] However, it is currently impossible to completely satisfy both the biostratigraphic and chemostratigraphic correlations. A globally synchronous expression is incompatible with the lack of enrichment in $\delta^{13}C_{org}$ of the upper Hettangian in the SW UK sections. This observation, together with the occurrence of a correlation of δ^{13}C with facies, suggests that the isotopic enrichment is regional is extent. Nevertheless, both carbon cycle consideration, as well as similarity to other events (discussed below) argue for a global distribution. Indeed, if one assumes that $\delta^{13}C_{org}$ of the SW UK sections did not faithfully record the δ^{13}C of seawater (perhaps due to a strong local control due to highly stratified conditions, as suggested by *Bartolini et al.* [2012]), then a global enrichment in δ^{13}C within the Hettangian is permissible by the current biostratigraphy: one small positive excursion in the lower Hettangian (*P. planorbis* zone) and one larger one in the upper Hettangian (*S. angulata* zone).

[50] Because isotopically enriched pools of carbon are rare, we hypothesize that the most likely driver of isotopic enrichment was increased organic carbon burial. We interpret the more muted increase in $\delta^{13}C_{org}$ relative to $\delta^{13}C_{carb}$ to reflect some combination of contributions from extrabasinal carbon and contemporaneous environmental changes that functioned to increase the average fractionation between CO_2 and organic matter coincident with the increase in $\delta^{13}C_{carb}$.

[51] We speculate that elevated pCO_2 could have played a key role in driving both aspects of the isotopic record. Elevated temperatures and reduced ocean oxygenation would have contributed to increases in organic carbon preservation and primary productivity [*van Cappellen and Ingall*, 1994] driving up organic carbon burial. At the same time, an increase in pCO_2 would have contributed to an increase in the isotopic difference between carbonate and organic carbon. We further speculate that the associated changes in climate and ocean chemistry could account for the observed correlation of δ^{13}C with facies, and largely barren nature of the strata coinciding with the interval of isotopic enrichment.

[52] The most likely driver for increased pCO_2 was the continued emission of volatiles from the Central Atlantic Magmatic Province (CAMP [*Marzoli et al.*, 1999; *Hames et al.*, 2000; *Marzoli et al.*, 2004; *Nomade et al.*, 2007; *Verati et al.*, 2007]). Such an environmental perturbation would be consistent with independent proxies for elevated CO_2 levels above the Triassic-Jurassic boundary [*McElwain et al.*, 1999], and in association with CAMP volcanism [*Schaller et al.*, 2011].

[53] From a broader perspective, the protracted interval of ^{13}C enrichment that occurs above the extinction horizon is not unique. Many similarities exist between the Triassic-Jurassic events and carbon isotopic records, and other better studied Mesozoic events that are interpreted as global. Isotope excursions occur in association with

massive volcanism [*Pálfy and Smith*, 2000; *Snow et al.*, 2005; *Turgeon and Creaser*, 2008; *Tejada et al.*, 2009; *Adams et al.*, 2010], as do similar patterns of δ^{13}C variation over time: the Early Toarcian OAE is accompanied by negative and positive excursions [*Jenkyns*, 1988; *Jenkyns and Clayton*, 1997; *Hesselbo et al.*, 2000; *Kemp et al.*, 2005], the Early Aptian OAE1a (Selli event) is accompanied by a short negative followed by a prolonged positive excursion [*Menegatti et al.*, 1998; *Jenkyns and Wilson*, 1999], and the Cenomanian-Turonian OAE2 (Bonarelli event) is accompanied by a positive excursion [*Arthur et al.*, 1988; *Sageman et al.*, 2006; *Jarvis et al.*, 2006].

[54] In the last two examples evidence from stable Ca and Sr isotopes indicates elevated weathering coincident with the positive peaks [*Blättler et al.*, 2011]. This points at an additional possible test for the origin of the ^{13}C enrichment: if the interval of positive δ^{13}C coincided with a period of strongly elevated pCO_2, similar trends in weathering sensitive elements should occur coincidentally with the positive excursions, with a phase lag proportional to the difference between their residence times and that of carbon. A reversal in the protracted Norian to Pliensbachian decline in $^{87}Sr/^{86}Sr$ that occurs in the Hettangian [*Cohen and Coe*, 2007] is suggestive, but data from well resolved sections will help further test this hypothesis, as well as assist with global stratigraphic correlations.

Acknowledgments

[55] We would like to thank Jozsef Pálfy for helpful comments on a previous version of this manuscript. Comments from Alan J. Kaufman and an anonymous reviewer greatly improved this manuscript. ABD would like to thank the NSF Graduate Research Fellowship and the Stanford School of Earth Sciences McGee and Levorsen Grants for their generous funding.

References

Adamoli, I., A. Bigozzi, G. Ciarapica, S. Cirilli, L. Passeri, A. Romano, F. Duranti, and F. Venturi (1990), Upper Triassic bituminous facies and Hettangian pelagic facies in the Gran Sasso range, *Boll. Soc. Geol. Ital.*, *109*, 219–230.

Adams, D. D., M. T. Hurtgen, and B. B. Sageman (2010), Volcanic triggering of a biogeochemical cascade during Oceanic Anoxic Event 2, *Nat. Geosci.*, *3*, 201–204.

Arthur, M. A., W. E. Dean, and G. E. Claypool (1985), Anomalous ^{13}C enrichment in modern marine organic carbon, *Nature*, *315*, 216–218.

Arthur, M. A., W. E. Dean, and L. M. Pratt (1988), Geochemical and climatic effects of increased marine organic carbon burial at the Cenomanian/Turonian boundary, *Nature*, *335*, 714–717.

Barattolo, F., and R. Romano (2005), Shallow carbonate platform bioevents during the Upper Triassic-Lower Jurassic: An evolutive interpretation, *Boll. Soc. Geol. Ital.*, *124*, 123–142.

Bartolini, A., J. Guex, J. E. Spangenberg, B. Schoene, D. G. Taylor, U. Schaltegger, and V. Atudorei (2012), Disentangling the Hettangian carbon isotope record: Implications for the aftermath of the end-Triassic mass extinction, *Geochem. Geophys. Geosyst.*, *13*, Q01007, doi:10.1029/2011GC003807.

Beerling, D. J., and R. A. Berner (2002), Biogeochemical constraints on the Triassic-Jurassic boundary carbon cycle event, *Global Biogeochem. Cycles*, *16*(3), 1036, doi:10.1029/2001GB001637.

Bertinelli, A., C. Nannarone, L. Passeri, and F. Venturi (2004), Hettangian ammonites and radiolarians in the Mt. Camicia (Gran Sasso, Central Apennines), *Riv. Ital. Paleontol. Stratigr.*, *110*, 87–96.

Bertinelli, A., G. Ciarpica, and L. Passeri (2005), Late Triassic-Jurassic basinal successions in Molise and northern Basilicata: The northernmost witness of the Ionian Ocean, *Boll. Soc. Geol. Ital.*, *124*, 177–188.

Bice, D. M., C. R. Newton, S. McCauley, P. W. Reiners, and C. A. McRoberts (1992), Shocked quartz at the Triassic-Jurassic boundary in Italy, *Science*, *255*, 443–446.

Bidigare, R. R., et al. (1997), Consistent fractionation of 13C in nature and in the laboratory: Growth-rate effects in some haptophyte algae, *Global Biogeochem. Cycles*, *11*, 279–292.

Blättler, C. L., H. C. Jenkyns, L. M. Reynard, and G. M. Henderson (2011), Significant increases in global weathering during Oceanic Anoxic Events 1a and 2 indicated by calcium isotopes, *Earth Planet. Sci. Lett.*, *309*, 77–88.

Bonis, N. R., W. M. Kürschner, and L. Krystyn (2009), A detailed palynological study of the Triassic-Jurassic transition in key sections of the Eiberg Basin (northern Calcareous Alps, Austria, *Rev. Palaeobot. Palynol.*, *156*, 376–400.

Bonis, N. R., M. Ruhl, and W. M. Kürschner (2010), Climate change driven black shale deposition during the end-Triassic in the western Tethys, *Palaeogeogr. Palaeoclimatol. Palaeoecol.*, *290*, 151–159.

Broecker, W., T. Peng (1982), *Tracers in the Sea*, Lamont-Doherty Geol. Obs., Columbia Univ., Palisades, N. Y.

Chiocchini, M., A. Farinacci, A. Mancinelli, V. Molinari, and M. Potetti (1994), Biostratigrafia a Foraminiferi, Dasicladali e Calpionelle delle Successioni Carbonatiche Mesozoiche dell'Appennino Centrale (Italia), in *Studi Geologici Camerti volume speciale: Biostratigraphia dell'Italia centrale*, pp. 9–129, Univ. di Camerino, Camerino, Italy.

Ciarapica, G. (2007), Regional and global changes around the Triassic-Jurassic boundary reflected in the late Norian-Hettangian history of the Apennine basins, *Palaeogeogr. Palaeoclimatol. Palaeoecol.*, *244*, 34–51.

Ciarapica, G., and L. Passeri (1980), La litostratigrafia della serie triassica del promontorio occidentale del Golfo di La Spezia, *Mem. Soc. Geol. Ital.*, *21*, 51–61.

Ciarapica, G., and L. Passeri (2005), Ionian tethydes in the southern Apennines, in *CROP Project: Deep Seismic Exploration of the Central Mediterranean and Italy*, pp. 209–224, Elsevier, Amsterdam.

Clémence, M. E., A. Bartolini, S. Gardin, G. Paris, V. Beaumont, and K. N. Page (2010), Early Hettangian benthic–planktonic coupling at Doniford (SW England): Palaeoenvironmental implications for the aftermath of the end-Triassic crisis, *Palaeogeogr. Palaeoclimatol. Palaeoecol.*, *295*, 102–115.

Cohen, A. S., and A. L. Coe (2007), The impact of the Central Atlantic Magmatic Province on climate and on the Sr- and

Os-isotope evolution of seawater, *Palaeogeogr. Palaeoclimatol. Palaeoecol.*, *244*, 374–390.

Deenen, M. H. L., M. Ruhl, N. R. Bonis, W. Krijgsman, W. M. Kuerschner, M. Reitsma, and M. J. van Bergen (2010), A new chronology for the end-Triassic mass extinction, *Earth Planet. Sci. Lett.*, *291*, 113–125.

Deuser, W. G. (1970), Extreme $^{13}C/^{12}C$ variations in quaternary dolomites from the continental shelf, *Earth Planet. Sci. Lett.*, *8*, 118–124.

Fazzuoli, M. (1974), Caratteri sedimentologici del Carcare Massiccio nell' area della Pania di Corfino (Provincia di Lucca), *Boll. Soc. Geol. Ital.*, *93*, 735–752.

Fazzuoli, M., and L. Orti (2006), The birth of Jurassic: From the sea or from the sky? Evidences from the northern Apennines (Italy), *Vol. Jurassica*, *4*, 279.

Fazzuoli, M., and L. Orti (2009), Remarks on the supposed bolid impacts at the T/J boundary in the Corfino Section (northern Apennines, Italy), *Vol. Jurassica*, *7*, 3–8.

Fazzuoli, M., E. Fois, and A. Turi (1988), Stratigraphia e Sedimentologia dei "Calcari e Marne a Rhaetivicula contorta" (Norico-Retico) della Toscana Nord-Occidentale—Nuova suddivisione formazionale, *Riv. Ital. Paleontol. Stratigr.*, *94*, 561–618.

Fiebig, J., B. R. Schöne, and W. Oschmann (2005), High-precision oxygen and carbon isotope analysis of very small (10–30 μg) amounts of carbonates using continuous flow isotope ratio mass spectrometry, *Rapid Commun. Mass Spectr.*, *19*, 2355–2358.

Freeman, K. H., J. M. Hayes (1992), Fractionation of carbon isotopes by phytoplankton and estimates of ancient CO_2 levels, *Global Biogeochem. Cycles*, *6*, 185–198.

Gaetani, M. (1970), Faune Hettangiane della parte orientale della provincia di Bergamo, *Riv. Ital. Paleontol. Stratigr.*, *76*, 355–442.

Galli, M. T., F. Jadoul, S. M. Bernasconi, and H. Weissert (2005), Anomalies in global carbon cycling and extinction at the Triassic/Jurassic boundary: Evidence from a marine C-isotope record, *Palaeogeogr. Palaeoclimatol. Palaeoecol.*, *216*, 203–214.

Galli, M. T., F. Jadoul, S. M. Bernasconi, S. Cirilli, and H. Weissert (2007), Stratigraphy and palaeoenvironmental analysis of the Triassic-Jurassic transition in the western southern Alps (northern Italy), *Palaeogeogr. Palaeoclimatol. Palaeoecol.*, *244*, 52–70.

Gischler, E., P. K. Swart, and A. J. Lomanodo (2009), Stable isotopes of carbon and oxygen in modern sediments of carbonate platforms, barrier reefs, atolls and ramps: Patterns and implications, *Int. Assoc. Sedimentol. Spec. Publ.*, *41*, 61–74.

Golonka, J. (2007), Late Triassic and Early Jurassic palaeogeography of the world, *Palaeogeogr. Palaeoclimatol. Palaeoecol.*, *244*, 297–307.

Guex, J., A. Bartolini, V. Atudorei, and D. Taylor (2004), High-resolution ammonite and carbon isotope stratigraphy across the Triassic-Jurassic boundary at New York Canyon (Nevada), *Earth Planet. Sci. Lett.*, *225*, 29–41.

Guex, J., B. Schoene, A. Bartolini, J. Spangenberg, U. Schaltegger, L. O'Dogherty, D. Taylor, H. Bucher, and V. Atudorei (2012), Geochronological constraints on post-extinction recovery of the ammonoids and carbon cycle perturbations during the Early Jurassic, *Palaeogeogr. Palaeoclimatol. Palaeoecol.*, *346–347*, 1–11.

Hallam, A. (1981), The end-Triassic bivalve extinction event, *Palaeogeogr. Palaeoclimatol. Palaeoecol.*, *35*, 1–44.

Hallam, A. (1994), Strontium isotope profiles of Triassic-Jurassic boundary sections in England and Austria, *Geology*, *22*, 1079–1082.

Hames, W. E., P. R. Renne, and C. Ruppel (2000), New evidence for geologically instantaneous emplacement of earliest Jurassic Central Atlantic magmatic province basalts on the North American margin, *Geology*, *28*, 859–862.

Hautmann, M., M. J. Benton, and A. Tomašových (2008), Catastrophic ocean acidification at the Triassic-Jurassic boundary, *Neues Jahrb. Geol. Palaeontol.*, *249*, 119–127.

Hayes, J. M., B. N. Popp, R. Takigiku, and M. W. Johnson (1989), An isotopic study of biogeochemical relationships between carbonates and organic carbon in the Greenhorn Formation, *Geochim. Cosmochim. Acta*, *53*, 2961–2972.

Hayes, J. M., H. Strauss, and A. J. Kaufman (1999), The abundance of ^{13}C in marine organic matter and isotopic fractionation in the global biogeochemical cycle of carbon during the past 800 Ma, *Chem. Geol.*, *161*, 103–125.

Hesselbo, S. P., D. R. Grocke, H. C. Jenkyns, C. J. Bjerrum, P. Farrimond, H. S. M. Bell, and O. R. Green (2000), Massive dissociation of gas hydrate during a Jurassic oceanic anoxic event, *Nature*, *406*, 392–395.

Hesselbo, S. P., S. A. Robinson, F. Surlyk, and S. Piasecki (2002), Terrestrial and marine extinction at the Triassic-Jurassic boundary synchronized with major carbon-cycle perturbation: A link to initiation of massive volcanism?, *Geology*, *30*, 251–254.

Hesselbo, S. P., S. A. Robinson, and F. Surlyk (2004), Sea-level change and facies development across potential Triassic-Jurassic boundary horizons, SW Britain, *J. Geol. Soc.*, *161*, 365–379.

Hollander, D. J., and J. A. McKenzie (1991), CO_2 control on carbon-isotope fractionation during aqueous photosynthesis: A paleo-pCO_2 barometer, *Geology*, *19*, 929–932.

Hounslow, M. W., P. E. Posen, and G. Warrington (2004), Magnetostratigraphy and biostratigraphy of the Upper Triassic and lowermost Jurassic succession, St. Audrie's Bay, UK, *Palaeogeogr. Palaeoclimatol. Palaeoecol.*, *213*, 331–358.

Jadoul, F., and M. T. Galli (2008), The Hettangian shallow water carbonates after the Triassic/Jurassic biocalcification crisis: The Albenza formation in the western Southern Alps, *Riv. Ital. Paleontol. Stratigr.*, *114*, 453–470.

Jadoul, F., M. T. Galli, L. Calabrese, and M. Gnaccolini (2005), Stratigraphy of Rhaetian to Lower Sinemurian carbonate platforms in western central Lombardy (southern Alps, Italy): Paleogeographic implications, *Riv. Ital. Paleontol. Stratigr.*, *111*, 285–303.

Jarvis, I., A. S. Gale, H. C. Jenkyns, and M. A. Pearce (2006), Secular variation in Late Cretaceous carbon isotopes: A new $\delta^{13}C$ carbonate reference curve for the Cenomanian-Campanian (99.6–70.6 Ma), *Geol. Mag.*, *143*, 561–608.

Jenkyns, H. C. (1988), The early Toarcian (Jurassic) anoxic event: Stratigraphic, sedimentary and geochemical evidence, *Am. J. Sci.*, *288*, 101–151.

Jenkyns, H. C., and C. J. Clayton (1997), Lower Jurassic epicontinental carbonates and mudstones from England and Wales: Chemostratigraphic signals and the early sToarcian anoxic event, *Sedimentology*, *44*, 687–706.

Jenkyns, H. C., and P. A. Wilson (1999), Stratigraphy, paleoceanography, and evolution of Cretaceous Pacific guyots: Relics from a greenhouse Earth, *Am. J. Sci.*, *299*, 341–392.

Johnston, D. T., F. A. Macdonald, B. C. Gill, P. F. Hoffman, and D. P. Schrag (2012), Uncovering the Neoproterozoic carbon cycle, *Nature*, *483*, 320–323.

Junge, C. E., M. Schidlowski, R. Eichmann, and H. Pietrek (1975), Model calculations for the terrestrial carbon cycle: Carbon isotope geochemistry and evolution of photosynthetic oxygen, *J. Geophys. Res.*, *80*, 4542–4552.

Kaufman, A. J., and S. Xiao (2003), High CO_2 levels in the Proterozoic atmosphere estimated from analyses of individual microfossils, *Nature*, *425*, 279–282.

Kemp, D. B., A. L. Coe, A. S. Cohen, and L. Schwark (2005), Astronomical pacing of methane release in the Early Jurassic period, *Nature*, *437*, 396–399.

Knoll, A. H., J. M. Hayes, A. J. Kaufman, K. Swett, and I. B. Lambert (1986), Secular variation in carbon isotope ratios from Upper Proterozoic successions of Svalbard and East Greenland, *Nature*, *321*, 832–838.

Korte, C., S. P. Hesselbo, H. C. Jenkyns, R. E. M. Rickaby, and C. Spötl (2009), Palaeoenvironmental significance of carbon- and oxygen-isotope stratigraphy of marine Triassic-Jurassic boundary sections in SW Britain, *J. Geol. Soc.*, *166*, 431–445.

Kronecker, W. (1910), Zur Grenzsbestimmung zwischen Trias und Lias in den Sudalpen, *Zentralbl. Mineral. Geol. Palaeontol.*, *1910*, 548–555.

Kump, L. R., and M. A. Arthur (1999), Interpreting carbon-isotope excursions: Carbonates and organic matter, *Chem. Geol.*, *161*, 181–198.

Kuroda, J., R. S. Hori, K. Suzuki, D. R. Gröcke, and N. Ohkouchi (2010), Marine osmium isotope record across the Triassic-Jurassic boundary from a Pacific pelagic site, *Geology*, *38*, 1095–1098.

Kürschner, W. M., N. R. Bonis, and L. Krystyn (2007), Carbon-isotope stratigraphy and palynostratigraphy of the Triassic-Jurassic transition in the Tiefengraben section—Northern Calcareous Alps (Austria), *Palaeogeogr. Palaeoclimatol. Palaeoecol.*, *244*, 257–280.

Lakew, T. (1990), Microfacies and cyclic sedimentation of the Upper Triassic (Rhaetian) Calcare di Zu (southern Alps), *Facies*, *22*, 187–232.

Lakew, T. (1994), Diagenesis of a Rhaetian Patch Reef (Lombardian Basin, southern Alps), *Riv. Ital. Paleontol. Stratigr.*, *100*, 9–32.

Laws, E. A., B. N. Popp, R. R. Bidigare, M. C. Kennicutt, and S. A. Macko (1995), Dependence of phytoplankton carbon isotopic composition on growth rate and CO_{2aq}: Theoretical considerations and experimental results, *Geochim. Cosmochim. Acta*, *59*, 1131–1138.

Lindström, S., B. van de Schootbrugge, K. Dybkjær, G. K. Pedersen, J. Fiebig, L. H. Nielsen, and S. Richoz (2012), No causal link between terrestrial ecosystem change and methane release during the end-Triassic mass extinction, *Geology*, *40*, 531–534.

Lloyd, R. M. (1964), Variations in the oxygen and carbon isotope ratios of Florida Bay mollusks and their environmental significance, *J. Geol.*, *72*, 84–111.

Longridge, L. M., J. Palfy, P. L. Smith, and H. W. Tipper (2008), Middle and late Hettangian (Early Jurassic) ammonites from the Queen Charlotte Islands, British Columbia, Canada, *Rev. Paleobiol.*, *27*, 191–248.

Mancinelli, A., M. Chiocchini, R. A. Chiocchini, and A. Romano (2005), Biostratigraphy of Upper Triassic-Lower Jurassic carbonate platform sediments of the central-southern Apennines (Italy), *Riv. Ital. Paleontol. Stratigr.*, *111*, 271–283.

Marzoli, A., P. R. Renne, E. M. Piccirillo, M. Ernesto, G. Bellieni, and A. D. Min (1999), Extensive 200-million-year-old continental flood basalts of the Central Atlantic Magmatic Province, *Science*, *284*, 616–618.

Marzoli, A., et al. (2004), Synchrony of the central Atlantic magmatic province and the Triassic-Jurassic boundary climatic and biotic crisis, *Geology*, *32*, 973–976.

McElwain, J. C., D. J. Beerling, and F. I. Woodward (1999), Fossil plants and global warming at the Triassic-Jurassic boundary, *Science*, *285*, 1386–1390.

McRoberts, C. A. (1994), The Triassic-Jurassic ecostratigraphic transition in the Lombardian Alps, Italy, *Palaeogeogr. Palaeoclimatol. Palaeoecol.*, *110*, 145–166.

McRoberts, C. A., H. Furrer, and D. S. Jones (1997), Palaeoenvironmental interpretation of a Triassic-Jurassic boundary section from western Austria based on palaeoecological and geochemical data, *Palaeogeogr. Palaeoclimatol. Palaeoecol.*, *136*, 79–95.

Menegatti, A. P., H. Weissert, R. S. Brown, R. V. Tyson, P. Farrimond, A. Strasser, and M. Caron (1998), High-resolution δ^{13}C stratigraphy through the Early Aptian "Livello Selli" of the Alpine Tethys, *Paleoceanography*, *13*, 530–545.

Morante, R., and A. Hallam (1996), Organic carbon isotopic record across the Triassic-Jurassic boundary in Austria and its bearing on the cause of the mass extinction, *Geology*, *24*, 391–394.

Muttoni, G., D. V. Kent, F. Jadoul, P. E. Olsen, M. Rigo, M. T. Galli, and A. Nicora (2010), Rhaetian magneto-biostratigraphy from the southern Alps (Italy): Constraints on Triassic chronology, *Palaeogeogr. Palaeoclimatol. Palaeoecol.*, *285*, 1–16.

Nomade, S., K. B. Knight, E. Beutel, P. R. Renne, C. Verati, G. Féraud, A. Marzoli, N. Youbi, and H. Bertrand (2007), Chronology of the Central Atlantic Magmatic Province: Implications for the central Atlantic rifting processes and the Triassic-Jurassic biotic crisis, *Palaeogeogr. Palaeoclimatol. Palaeoecol.*, *244*, 326–344.

Pálfy, J., and P. L. Smith (2000), Synchrony between Early Jurassic extinction, oceanic anoxic event, and the Karoo-Ferrar flood basalt volcanism, *Geology*, *28*, 747–750.

Pálfy, J., and N. Zajzon (2012), Environmental changes across the Triassic–Jurassic boundary and coeval volcanism inferred from elemental geochemistry and mineralogy in the Kendlbachgraben section (Northern Calcareous Alps, Austria), *Earth Planet. Sci. Lett.*, *335–336*, 121–134.

Pálfy, J., A. Demeny, J. Haas, M. Hetenyi, M. J. Orchard, and I. Veto (2001), Carbon isotope anomaly and other geochemical changes at the Triassic-Jurassic boundary from a marine section in Hungary, *Geology*, *29*, 1047–1050.

Passeri, L., A. Bertinelli, and G. Ciarapica (2005), Paleogeographic meaning of the Late Triassic–Early Jurassic Lagonegro units, *Boll. Soc. Geol. Ital.*, *124*, 231–245.

Patterson, W. P., and L. M. Walter (1994), Depletion of ^{13}C in seawater ΣCO_2 on modern carbonate platforms: Significance for the carbon isotopic record of carbonates, *Geology*, *22*, 885–888.

Popp, B. N., E. A. Laws, R. R. Bidigare, J. E. Dore, K. L. Hanson, and S. G. Wakeham (1998), Effect of phytoplankton cell geometry on carbon isotopic fractionation, *Geochim. Cosmochim. Acta*, *62*, 69–77.

Ronchetti, C. R., and C. Brena (1953), Studi paleontologici sul Lias del Monte Albenza. Brachiopodi dell'Hettangiano, *Riv. Ital. Paleontol. Stratigr.*, *59*, 1–26.

Ruhl, M., and W. Kürschner (2011), Multiple phases of carbon cycle disturbance from large igneous province formation at the Triassic-Jurassic transition, *Geology*, *39*, 431–434.

Ruhl, M., W. M. Kürschner, and L. Krystyn (2009), Triassic-Jurassic organic carbon isotope stratigraphy of key sections in the western Tethys realm (Austria), *Earth Planet. Sci. Lett.*, *281*, 169–187.

Ruhl, M., M. H. L. Deenen, H. A. Abels, N. R. Bonis, W. Krijgsman, and W. M. Kürschner (2010a), Astronomical constraints on the duration of the early Jurassic Hettangian stage and recovery rates following the end-Triassic mass extinction (St Audrie's Bay/East Quantoxhead, UK), *Earth Planet. Sci. Lett.*, *295*, 262–276.

Ruhl, M., H. Veld, and W. M. Kürschner (2010b), Sedimentary organic matter characterization of the Triassic-Jurassic boundary GSSP at Kuhjoch (Austria), *Earth Planet. Sci. Lett.*, *292*, 17–26.

Ruhl, M., N. R. Bonis, G. J. Reichart, J. S. S. Damsté, and W. M. Kürschner (2011), Atmospheric carbon injection linked to end-Triassic mass extinction, *Science*, *333*, 430–434.

Sageman, B. B., S. R. Meyers, and M. A. Arthur (2006), Orbital timescale and new C-isotope record for Cenomanian-Turonian boundary stratotype, *Geology 34*, 125–128.

Schaller, M. F., J. D. Wright, and D. V. Kent (2011), Atmospheric pCO_2 perturbations associated with the Central Atlantic Magmatic Province, *Science*, *331*, 1404–1409.

Shinn, E. A., R. P. Steinen, B. H. Lidz, and P. K. Swart (1989), Whitings, a sedimentologic dilemma, *J. Sediment. Petrol.*, *59*, 147–161.

Snow, L. J., R. A. Duncan, and T. J. Bralower (2005), Trace element abundances in the Rock Canyon Anticline, Pueblo, Colorado, marine sedimentary section and their relationship to Caribbean plateau construction and oxygen anoxic event 2, *Paleoceanography*, *20*, PA3005, doi:10.1029/2004PA001093.

Spötl, C., and T. W. Vennemann (2003), Continuous-flow isotope ratio mass spectrometric analysis of carbonate minerals, *Rapid Commun. Mass Spectr.*, *17*, 1004–1006.

Stiller, M., J. S. Rounick, S. Shasha (1985), Extreme carbon-isotope enrichments in evaporating brines, *Nature*, *316*, 434–435.

Swart, P. K. (2008), Global synchronous changes in the carbon isotopic composition of carbonate sediments unrelated to changes in the global carbon cycle, *Proc. Natl. Acad. Sci.*, *105*, 13,741–13,745.

Tejada, M. L. G., K. Suzuki, J. Kuroda, R. Coccioni, J. J. Mahoney, N. Ohkouchi, T. Sakamoto, and Y. Tatsumi (2009), Ontong Java Plateau eruption as a trigger for the early Aptian oceanic anoxic event, *Geology*, *37*, 855–858.

Tipper, H. W., P. L. Smith, B. E. B. Cameron, E. S. Carter, G. K. Jakobs, and M. J. Johns (1991), Biostratigraphy of the Lower Jurassic formations of the Queen Charlotte Islands, British Columbia, in *Evolution and Hydrocarbon Potential of the Queen Charlotte Basin, British Columbia*, edited by G. J. Woodsworth, *Pap. Geol. Surv. Can.*, *90-10*, 203–235.

Turgeon, S. C., R. A. Creaser (2008), Cretaceous oceanic anoxic event 2 triggered by a massive magmatic episode, *Nature*, *454*, 323–326.

van Cappellen, P., and E. D. Ingall (1994), Benthic phosphorus regeneration, net primary production, and ocean anoxia: A model of the coupled marine biogeochemical cycles of carbon and phosphorus, *Paleoceanography*, *9*, 677–692.

van de Schootbrugge, B., F. Tremolada, Y. Rosenthal, T. R. Bailey, S. F. Burkhardt, H. Brinkhuis, J. Pross, D. V. Kent, and P. G. Falkowski (2007), End-Triassic calcification crisis and blooms of organic-walled 'disaster species,' *Palaeogeogr. Palaeoclimatol. Palaeoecol.*, *244*, 126–141.

van de Schootbrugge, B., J. L. Payne, A. Tomasovych, J. Pross, J. Fiebig, M. Benbrahim, K. B. Föllmi, and T. M. Quan (2008), Carbon cycle perturbation and stabilization in the wake of the Triassic-Jurassic boundary mass-extinction event, *Geochem. Geophys. Geosyst.*, *9*, Q04028, doi:10.1029/2007GC001914.

Verati, C., C. Rapaille, G. Féraud, A. Marzoli, H. Bertrand, and N. Youbi (2007), $^{40}Ar/^{39}Ar$ ages and duration of the Central Atlantic Magmatic Province volcanism in Morocco and Portugal and its relation to the Triassic-Jurassic boundary, *Palaeogeogr. Palaeoclimatol. Palaeoecol.*, *244*, 308–325.

Ward, P. D., J. W. Haggart, E. S. Carter, D. Wilbur, H. W. Tipper, and T. Evans (2001), Sudden productivity collapse associated with the Triassic-Jurassic boundary mass extinction, *Science*, *292*, 1148–1151.

Ward, P. D., G. H. Garrison, J. W. Haggart, D. A. Kring, and M. J. Beattie (2004), Isotopic evidence bearing on Late Triassic extinction events, Queen Charlotte Islands, British Columbia, and implications for the duration and cause of the Triassic/Jurassic mass extinction, *Earth Planet. Sci. Lett.*, *224*, 589–600.

Ward, P. D., G. H. Garrison, K. H. Williford, D. A. Kring, D. Goodwin, M. J. Beattie, and C. A. McRoberts (2007), The organic carbon isotopic and paleontological record across the Triassic–Jurassic boundary at the candidate GSSP section at Ferguson Hill, Muller Canyon, Nevada, USA, *Palaeogeogr. Palaeoclimatol. Palaeoecol.*, *244*, 281–289.

Williford, K. H., P. D. Ward, G. H. Garrison, and R. Buick (2007), An extended organic carbon-isotope record across the Triassic-Jurassic boundary in the Queen Charlotte Islands, British Columbia, Canada, *Palaeogeogr. Palaeoclimatol. Palaeoecol.*, *244*, 290–296.

Williford, K. H., J. Foriel, P. D. Ward, and E. J. Steig (2009), Major perturbation in sulfur cycling at the Triassic-Jurassic boundary, *Geology*, *37*, 835–838.

Zappaterra, E. (1994), Source-rock distribution model of the Periadriatic region, *AAPG Bull.*, *78*, 333–354.

Zeebe, R. E., and D. Wolf-Gladrow (2001), *CO_2 in Seawater: Equilibrium, Kinetics, Isotopes*, *Oceanogr. Ser.*, vol. 65, Elsevier, Amsterdam.